

博士学位請求論文

論文題目 A study of cell proliferation and neurogenesis
by 532 nm low-power laser irradiation

専攻名 生命情報工学専攻

学籍番号 12D5604

氏名 福崎 由美

指導教員 木暮 信一

創価大学大学院
工学研究科

**A study of cell proliferation and neurogenesis
by 532 nm low-power laser irradiation**

2015 年 8 月

福崎 由美

Table of contents

Chapter 1. Introduction

1.1 Category and property of the light	pp.2–3
1.2 Laser	pp.4–6
1.3 Low-power laser irradiation (LLI) treatment	pp.7–8
1.4 Effect of LLI on intracellular mechanism	pp.9–11
1.5 Cell types for experiment of LLI	p.12
1.5.1 Glioblastoma A-172 cells	pp.13–14
1.5.2 Effect of γ -secretase inhibitor (GSI) on Notch and APP	pp.15–17
1.5.3 Embryonic neural stem/progenitor cells (NSPCs)	pp.18–19
1.5.4 Adult NSPCs	pp.20–22
1.6 References	pp.23–28

Chapter 2. Effect of 532 nm LLI promoted the proliferation of Glioblastoma A-172

2.1 Introduction	p.30
2.2 Materials and Methods	
2.2.1 Cell culture of Glioblastoma (A-172)	p.30
2.2.2 Laser irradiation method	p.31
2.2.3 Cell counting by microscopic observations	p.32
2.2.4 Cell Viability by MTT Assay	p.32

2.2.5	Analysis of ATP Level in Cell Lysate	· · · · ·	p.32
2.2.6	Statistical analysis	· · · · ·	p.32
2.3	Results		
2.3.1	Effects of 532 nm LLI on the Number of A-172 Cells	· · ·	pp.34–35
2.3.2	ATP Level in Cell Lysates	· · · · ·	pp.36
2.4	Discussion	· · · · ·	p.37
2.5	References	· · · · ·	p.38

Chapter 3. 532 nm LLI Recovers γ -Secretase Inhibitor-Mediated Cell Growth Suppression and Promotes Cell Proliferation via Akt Signaling

3.1	Introduction	· · · · ·	p.40
3.2	Materials and Methods		
3.2.1	Immunofluorescent staining method	· · · · ·	p.40
3.2.2	Pretreatment Cells with γ -secretase Inhibitor (GSI)	· · ·	p.41
3.2.3	Laser Irradiation Method	· · · · ·	p.41
3.2.4	Cell Culture of Glioblastoma (A-172)	· · · · ·	p.41
3.2.5	Statistical analysis	· · · · ·	p.42
3.3	Results		
3.3.1	Expressions of p-Akt and p-PTEN by 532 nm LLI	· · ·	pp.42–43
3.3.2	Effects of a combined application of GSI and LLI on cell proliferation	· ·	p.44
3.3.3	Effects of LLI on Intracellular Signaling Molecules under GSI	· ·	pp.45–46
3.4	Discussion	· · · · ·	p.47
3.5	References	· · · · ·	pp.48–49

Chapter 4. 532 nm LLI facilitates migration on NSPCs derived from E14 GE whereas promotes proliferation on NSPCs derived E10 FB

4.1 Introduction p.51

4.2 Materials and Methods

 4.2.1 Neural Stem/Progenitor Cell (NSPC) primary culture pp.51–52

 4.2.2 Proliferation analysis and migration analysis in culture p.52

 4.2.3 Western blotting p.53

 4.2.4 Laser irradiation method p.54

 4.2.5 Statistical Analysis p.54

4.3 Results

 4.3.1 LLI effect on cell proliferation of cultured NSPCs derived from E10 forebrain pp.55–56

 4.3.2 LLI effect on cell migration of cultured NSPCs derived from E14 MGE p.55, p.57

 4.3.3 LLI effect on pAkt and Akt expression of cultured cells p.58

4.4 Discussion p.59

4.5 References p.60

Chapter 5. 532 nm LLI facilitates migration of GAD67 positive NSPCs in adult neocortex

5.1 Introduction p.62

5.2 Materials and Methods

5.2.1 Transient mild ischemia · · · · ·	pp.62–63
5.2.2 Laser Irradiation Method · · · · ·	p.64
5.2.3 Triphenyltetrazolium ^{III} staining · · · · ·	p.65
5.2.4 Western blot analysis	
5.2.5 Immunohistochemistry · · · · ·	pp.66–67
5.2.6 Statistical Analysis · · · · ·	p.67
5.3 Results	
5.3.1 Effects of transcranial LLI on cell migration of NSPCs induced by CCAO · · · · ·	pp.68–70
5.3.2 Effects of transcranial LLI on pAkt and Akt expression in mouse cortex · · · · ·	pp.70–71
5.4 Discussion · · · · ·	pp.72–73
5.5 References · · · · ·	p.74

Acknowledgment

謝辞 (日本語) · · · · ·	p.75
--------------------	------

Chapter 1

Introduction

Contents

- 1.1 Category and property of the light
 - 1.2 Laser
 - 1.3 Low-power laser irradiation (LLI) treatment
 - 1.4 Effect of LLI on intracellular mechanism
 - 1.5 Cell types for experiment of LLI
 - 1.5.1 Glioblastoma A-172 cells
 - 1.5.2 Effect of γ -secretase inhibitor (GSI) on Notch and APP
 - 1.5.3 Embryonic neural stem/progenitor cells (NSPCs)
 - 1.5.4 Adult NSPCs
 - 1.6 References
-

1.1 Category and property of the light

Isaac Newton, English physicist and mathematician, found that white light can be separated to different color with a prism in 1666¹⁾. These separated light is classified into visible light and invisible light. The wavelength of visible light is from 380 nm to 770 nm (Fig. 1A), which is responded as a color by a retina of human eyes²⁾. There are 3 types of retinal photoreceptors having cone photoreceptor: firstly the short-wavelength sensitive cones (S-cone), also known as blue cones, responded to around 440 nm, secondly the middle-wavelength sensitive cones (M-cone) or green cones responded to around 545 nm and finally the long-wavelength sensitive cones (L-cone) or red cones responded to around 565 nm (Fig. 1B). Based on human perception of colors, the blue, green and red are called RGB color model, which is principle for color lights (Fig. 1C). A monitor of electronic machine in modern society is shown based on RGB color model. Besides, the invisible lights, which are outside of visible light, are classified into 2 types: long wavelength from 700 nm to 1 mm is infrared (IR) light and short wavelength from 10 nm to 380 nm is ultraviolet (UV) light. William Herschel, a German-born British astronomer, discovered IR light by using prism in 1800³⁾. Currently, IR is used in heating source, thermometer and night vision equipment. Johann Wilhelm Ritter, a German physicist, discovered UV light by silver chloride in 1801³⁾. Effect of UV light is known as cause of skin cancer directly⁴⁾ and support of vitamin D production⁵⁾. In the out of invisible light, X-rays and Gamma rays exist in short wavelength, and microwaves and radio waves exist in long wavelength. These are not categorized into the light in general.

The light has characteristics both of waves and particles, which is called the “wave-particle duality”. Firstly, the light has the same property of radio wave. The different phenomena from radio wave are the light can gather and concentrate on one place and the light travels in a straight line. Secondly, the light has the same property of particle. The photon, particle of light, does not have any weight and electric charge. The energy of photon (E) are calculated by $E = hf$, where light frequency is denoted by f and planck constant is denoted by h . The energy of photon is inverse proportion: $hf = hc / \lambda$ where light wavelength is denoted by λ and light velocity is denoted by c . Therefore, the short wavelength of light is higher photon energy than long wavelength.

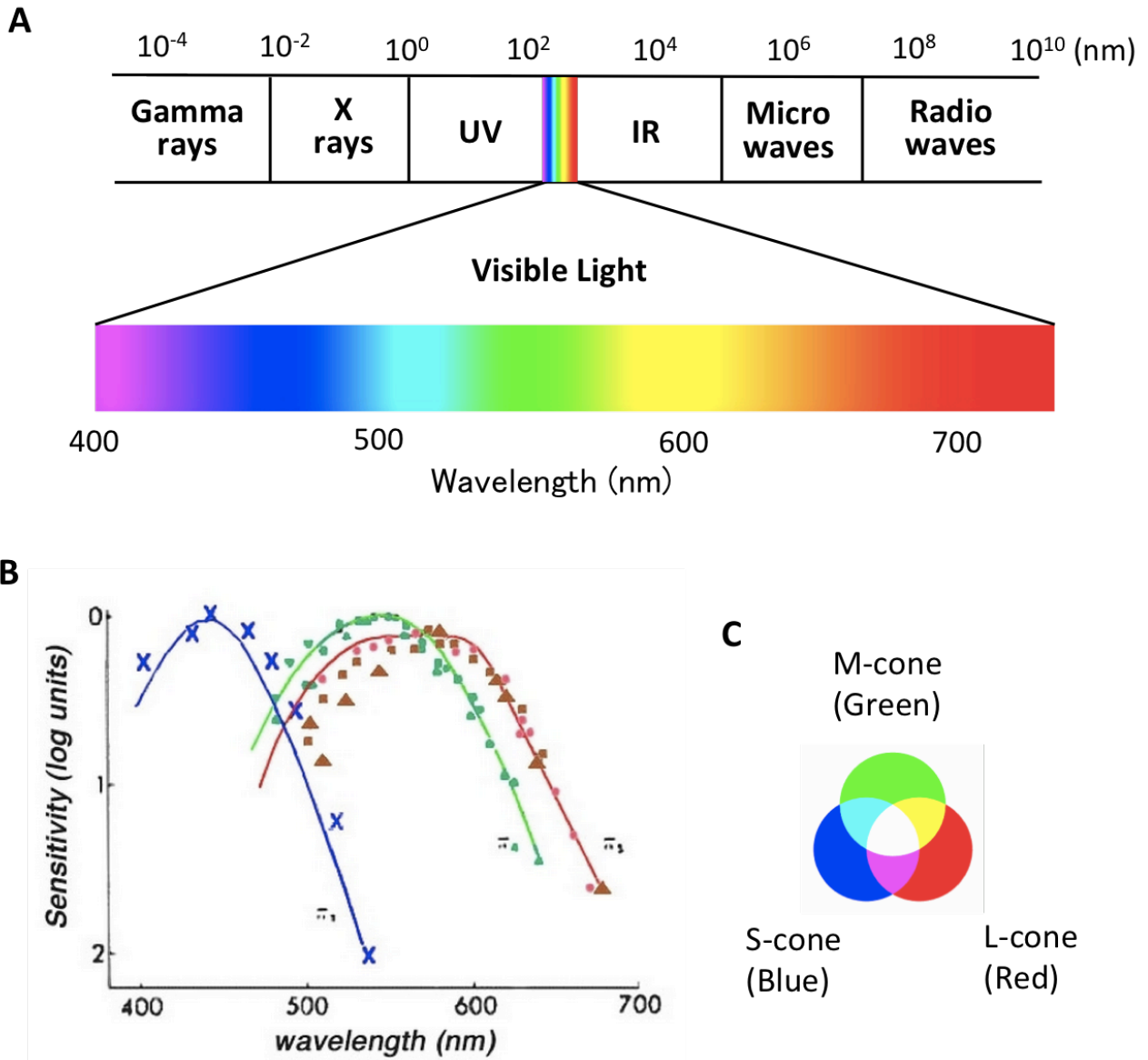


Fig. 1 (A) Relation between wavelength and color in the visible light. (B) Sensitivity of human retina. Blue is S-cone, Green is M-cone, and Red is L-cone (C) red-green-blue (RGB) model. The combine of all color make white color in the light. (Helga Kolb, et al., Webvision The organization of the retina and visual system, Part VIII, <http://webvision.med.utah.edu/>)

1.2 Laser

The fundamental laser oscillations (Fig. 2B) are the following process.

- 1) Pumping: excitation light supply energy to the laser gain medium
- 2) Spontaneous emission: photon is released from laser gain medium
- 3) Stimulated emission: photon derived from laser gain medium affect to excited electron
- 4) Light amplification: stimulated emission continues between two mirrors
- 5) Out put: laser output through the partially transparent mirror

The laser is an acronym for “light amplification by stimulated emission of radiation”, which was recognized in a published paper by Gordon Gould in 1959⁶⁾. Charles H. Townes, Nikolay Basov, and Aleksandr Prokhorov studied the basic principles of laser in the field of quantum electronics. They won the Nobel Prize for physics in 1964. The “stimulated emission” originating expresses principles of laser itself. From the establishment of Einstein's B coefficient, photon is absorbed to electron (stimulated absorption), and electron is excited. When these excited electron drop to the ground state from the excited state in natural, photons are released (spontaneous emission). If photon is absorbed at the same timing of spontaneous emission, two photons are released with identical wavelength, phase, and direction (stimulated emission) (Fig. 2A).

The light oscillated by laser contains unique properties differenced with the normal lights. Although “natural lights” from the Sun or the Moon include the color of all wavelengths, the laser can provide color of one wavelength with high intensity (monochromaticity light). The normal light including natural light and artificial light spread to all directions, but the wave of laser light travels to one direction (directivity light). The laser lights overlap the phase of wavelength at same timing (coherent light).

The laser oscillators are classified into either the continuous wave (CW) or the pulsed mode. The pulsed beam looks like CW beam because of the brief interval of pulses. The widths of pulse are nanoseconds (10^{-9} s), picoseconds (10^{-12} s) or femtoseconds (10^{-15} s). Pulsed laser can oscillate with high energy in short time, thus heat effect of laser is suppressed. Whereas CW

laser need to consider heat effect when applying to human body. The power is categorized to 2 groups: low-power laser irradiation (LLI) and high-power laser irradiation (HLI). The HLI is used as scalpel in a surgical operation. The laser scalpel can vaporize tissue in an instant. The bloods are coagulated by HLI immediately, thus the wounds of surgery are easy to recover. The areas of necrosis tissue by denaturation are smaller than electric scalpel. In addition, there are photothermal effect and photostimulating effect away from center of HLI (Fig. 2C)⁷. Photothermal effects induce Vaporization, Carbonization, Coagulation and Denaturation. The photostimulating effect is same as LLI, hence HLI include LLI stimulation. The effects of LLI on the tissue are described at *subsection 1.3*. in detail, but LLI should contribute to treat from surgery by HLI scalpel.

When laser irradiates to the body of human, how far the light reach in the tissue? The invasion depths of tissue depend on wavelength: the short-wavelength was low permeability and long-wavelength was high permeability. The permeability of light is mainly caused by absorption characteristics of hemoglobin and light-scattering property. P.Beard reviewed the absorption coefficient spectra of endogenous component⁸: Oxyhaemoglobin, deoxyhaemoglobin, water, lipid, melanin, collagen and protein of elastin (Fig.2D). The haemoglobin absorption coefficients in the region of Red and IR are less than other visible light. AE. Te showed that the 1064 nm laser penetrates skin tissue (10 mm) twice as deep as the 830 nm laser (5 mm), and 10 times more than the 532 nm laser (0.8 mm)⁹. Hence, long wavelengths are suited for irradiation of deep tissue, and short wavelengths are suitable for superficial region or small area. In addition, the permeability is different on type of the tissue. For example, permeability of the gray matter in the brain is twice as high as the white matter¹⁰.

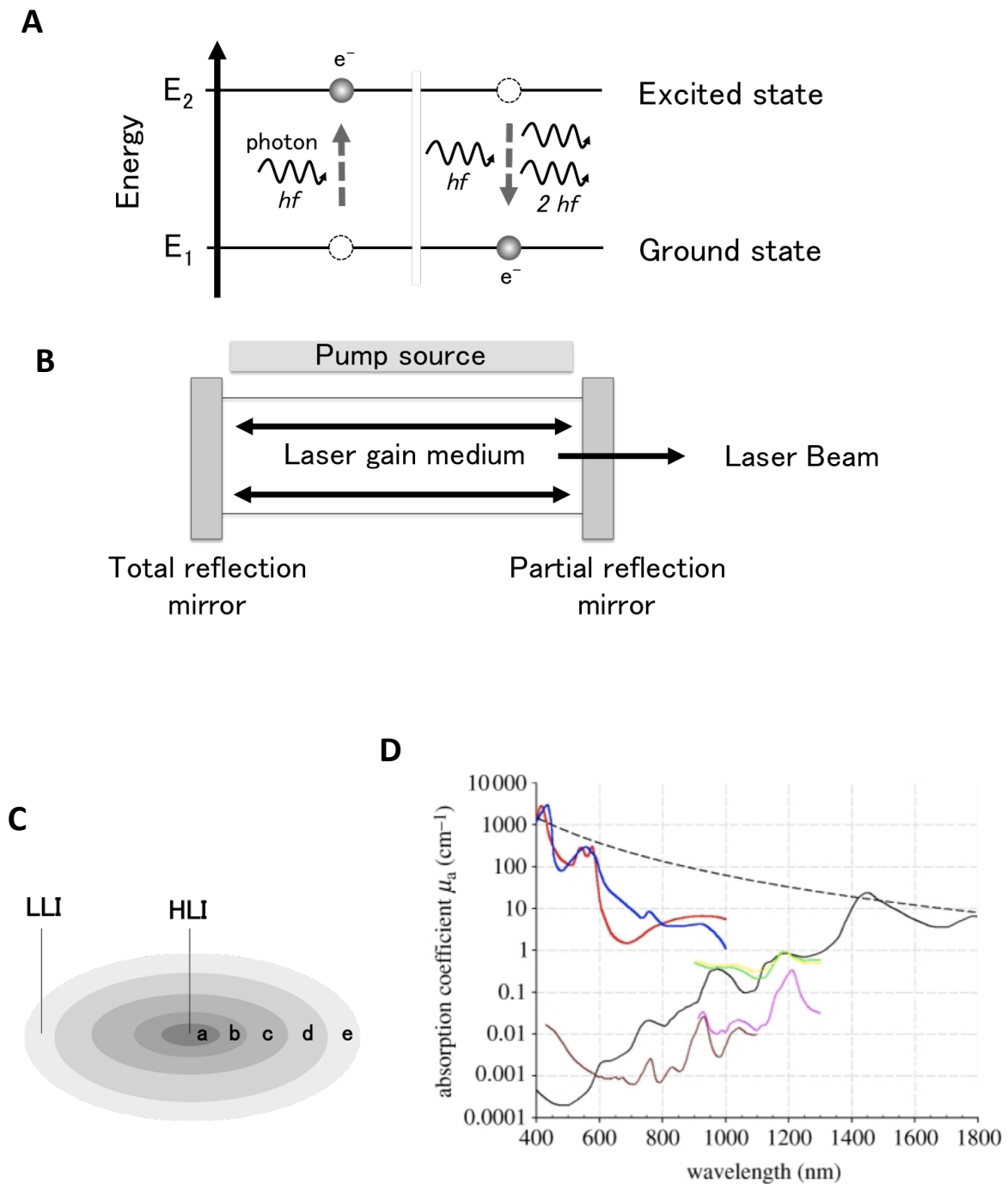


Fig. 2 (A) Principle of the stimulated emission. f :Frequency, h :Planck constant. (B) The structure of the laser instrument. The arrow showed the light path. (C) Feature of HLI. a: Vaporization, b:Carbonization, c: Coagulation, d:Denaturation, e: Photostimulating effect. (D) The absorption characteristics of the light. Red line: Oxyhaemoglobin (HbO_2), blue line: deoxyhaemoglobin (HHb), black line: water, brown line:lipid(a), pink line: lipid(b), black dashed line:melanin, green line:Collagen and yellow line: elastin. (From Beard P, Interface Focus.1-4:602–31, 2011)

1.3 Low-power laser irradiation (LLI) treatment

It has been reported that the low-power laser irradiation (LLI) can promote cell proliferation and survival. Endre Mester (1903-1984), a Hungarian physician, started LLI research in 1965, a few years after laser was invented. First, he investigated the question of whether LLI would cause tumor or not. The newly-developed ruby laser (694 nm) irradiated to the shaven mice. Contrary to his expectations, the LLI did not cause tumor but LLI facilitated hair-growth on irradiation group compared with control group. In next LLI experiment, he examined using intractable skin tumor implanted in mice. In his published paper in 1968, LLI facilitated healing of dissection sites. Presently, Tina Karu is one of famous scientist in modern field of LLI, she wrote 3 books about LLI: “*Photobiology of Low-Power Laser Therapy*” (Chur, London, Paris, New York: Harwood Academic Publ., 1989), “*The Science of Low Power Laser Therapy*” (London: Gordon and Breach Sci. Publ., ISBN 90-5699108.6, 1998) and “*Ten Lectures on Basic Science of Laser Phototherapy*” (Prima Books AB, Grängesberg, Sweden, 2007). She has met E.Mester at a laser conference in Florence, Italy, in 1979 and listened to his presentation about the healing of leg ulcerations with LLI. And she gave her impressions on the Mester’s lecture: “The patients had failed to respond to traditional medicine, and were cured with the Low Level Light Therapy. It was a striking example of the photostimulation of wound healing.” Ever since these biological effects of LLI were discovered, there are many reports demonstrating effective LLI treatment in various fields including wound healing, rheumatoid arthritis¹³⁾, tendinopathy¹⁴⁾, osteoarthritis¹⁵⁾.

Red-to-IR laser treatments are also called LLLT: low-level laser therapy. Red laser was made as the first commercially instrument. And the property of permeability in Red and IR laser, thus most reports of laser therapy indicate treatment by irradiation of Red-to-IR. Oron et al. reported 880 nm LLI decreased neurological deficits and increased neurogenesis in the subventricular zone after acute stroke by permanent middle cerebral artery occlusion in rats¹⁶⁾. Recently, 808 nm LLI therapy showed initial safety and effective keep as a new treatment strategy for human ischemic stroke¹⁷⁾. Zhang et al. showed that 810 nm LLI not only inhibited inflammatory mediators generated by gentle traumatic brain injury but also dramatically

inhibited secondary brain injury in mice lacking immediate early response gene X-1¹⁸⁾.

In cell culture systems, Red-to-IR LLI was different effects on proliferation of diverse cells. The increasing proliferations by Red-to-IR LLI occur in the following cells: 632.8 nm LLI on human skin fibroblast¹⁹⁾, 633 nm LLI on rabbit articular chondrocytes²⁰⁾, 660 nm LLI on lymphocytes²¹⁾, 625, 635, 645, 655, 665 and 675 nm on fibroblasts and endothelial cells²²⁾, 635 and 805 nm on normal urothelial cells and urothelial carcinoma cells²³⁾, whereas the decreasing proliferations by Red-to-IR LLI occur in the following cells: 805 nm LLI on glioblastoma cells (U373MG cell line), mamma adenocarcinoma cells and human squamous carcinoma cells of the gingival mucosa²³⁾, 808 nm on human hepatoma cells²⁴⁾ and 810 nm on fibroblasts and endothelial cells²²⁾.

The efficacy of LLI treatment focused on other different wavelength accompanied with the development of laser instrument for Blue and Green light. The effects of LLI in the Red (632.8 nm), Green (532 nm), and Blue (441.2 nm) were studied on wound healing in rats¹⁹⁾. The shaved skin 10 mm in diameter was cut with scissors before LLI treatment. With the fluence of LLI at 0.75 J/cm², 441.2 nm LLI decreased injury area 53% compared with control; 532 nm LLI decreased 33% and 632.8 nm LLI decreased 39% at day 15 after the injury. At 1.5 J/cm², 441.2 nm LLI decreased 39%, 532 nm LLI decreased 20% and 632.8 nm LLI decreased 75% compared with injury area of control at day 15²⁵⁾.

In cell culture systems using other wavelength LLIs, we can find reports showing that 532 nm LLI promoted proliferation of B-14 (Chinese hamster ovarian cell line) cells without inducing cell death²⁶⁾, it influenced blood platelets to trigger signal transduction, leading to platelet activation²⁷⁾, and it significantly increased cell survival of human adipose tissue-derived stem cells following mitochondria activation²⁸⁾.

1.4 Effect of LLI on intracellular mechanism

Different effects of LLI wavelength on cell proliferation and survival may depend on photoacceptors present in mitochondria, especially those in the mitochondrial respiratory chain²⁹. Primary photoacceptors include cytochromes c oxidase, another name is complex IV, for absorption of red and IR light region, NADH-dehydrogenase, complex I, for absorption of blue spectral region, and cytochromes b, c1 and c, complex III and cytochrome c for absorption of green light region (Table 1). Their cofactors are porphyrins (for cytochrome c oxidase and cytochromes b, c1 and c), or flavins (for NADH-dehydrogenase), respectively³⁰. These photoreceptors and cofactors contribute to the generation of ATP, a critical source of chemical energy in cells. Mitochondria are the center of many diverse cellular functions such as signaling, cellular differentiation, cell death, as well as the control of the cell cycle and cell growth³¹. Thus photoacceptors in mitochondria upon light absorption may regulate the level of ATP to support cell survival.

It has been reported LLI increased the amount of the intracellular ATP. 830 nm LLI increased ATP without any to ADP³²) in the rat brain tissue. But 652 nm LLI showed no effect on both ATP and ADP³²). 810 nm LLI increased the ATP level on cultured mouse cortical neurons at 3 J/cm², whereas LLI of higher fluence at 10 and 30 J/cm² were equal to the ATP level of non-irradiated control³³). In other work using Hela cell line, the human cervical cancer cell line, 820 nm LLI (1 J/cm²) decreased ATP level³⁴) and 632.8 nm LLI (0.01 J/cm²) increased the ATP level at 20 min after irradiation and decreased it slowly to control level³⁵).

Table 1

Cofactors	Photo acceptor		Wavelength
Porphyrins	Cytochromes c oxidase	Complex I	Red-IR
	Cytochromes b, c1 and c	Complex III, Cytochrome C	Green
Flavins	NADH-dehydrogenase	Complex IV	Blue

However, considering that LLI has different biological effects on different cells, it is difficult to conceive that the regulation of mitochondrial photoacceptors is the only mechanism underlying LLI-mediated cell proliferation. It is likely that final consequences of specific photobiological effects for cell proliferation are determined not at the level of reactions in the mitochondrial respiratory chain but based on intracellular signaling²⁹). It will be important to characterize how proteins and enzymes expressed in each cell type contribute to photobiological effects.

Akt plays a key role for cell survival and proliferation³⁶). It was demonstrated that 632 nm LLI increased cell proliferation via the activation of Akt signaling pathway³⁷). And 632.8 nm LLI inhibits the expression of p21³⁸), a molecule that arrests the cell-cycle, and enhances the cell-cycle progress via its phosphorylation by Akt³⁹). Recent investigations implicate an important role of Akt in mitochondria for the regulation of cell growth. The expression level of Akt in mitochondria is dynamically regulated by cellular signaling activities⁴⁰), and Akt mediates mitochondrial protection against cell death induced by ischemia in cardiomyocytes⁴¹). Importantly, mitochondria-targeted active Akt suppresses apoptosis signaling independent of cytosolic Akt in cardiac muscle cells⁴²). Fig. 3 showed mechanism of apoptosis signaling via mitochondria. When the protein of BH123 aggregated in mitochondria membrane, Cytochrome C is released from mitochondria. Cytochrome C activates the caspase 9 with Apf1. Caspase 9 make a apoptosome and activate caspase 3, which is the final protein for apoptosis. The recent work using 632.8 nm LLI indicated that Akt activation is involved in prevention of cell apoptosis⁴³). Another work using 660 nm LLI showed that the expression of pro-apoptotic factors (caspase 3 and caspase 9) were decreased while expression of antiapoptotic factors, such as Akt, pAkt, Bcl-2 and pBAD were increased by LLI, following transient cerebral ischemia⁴⁴).

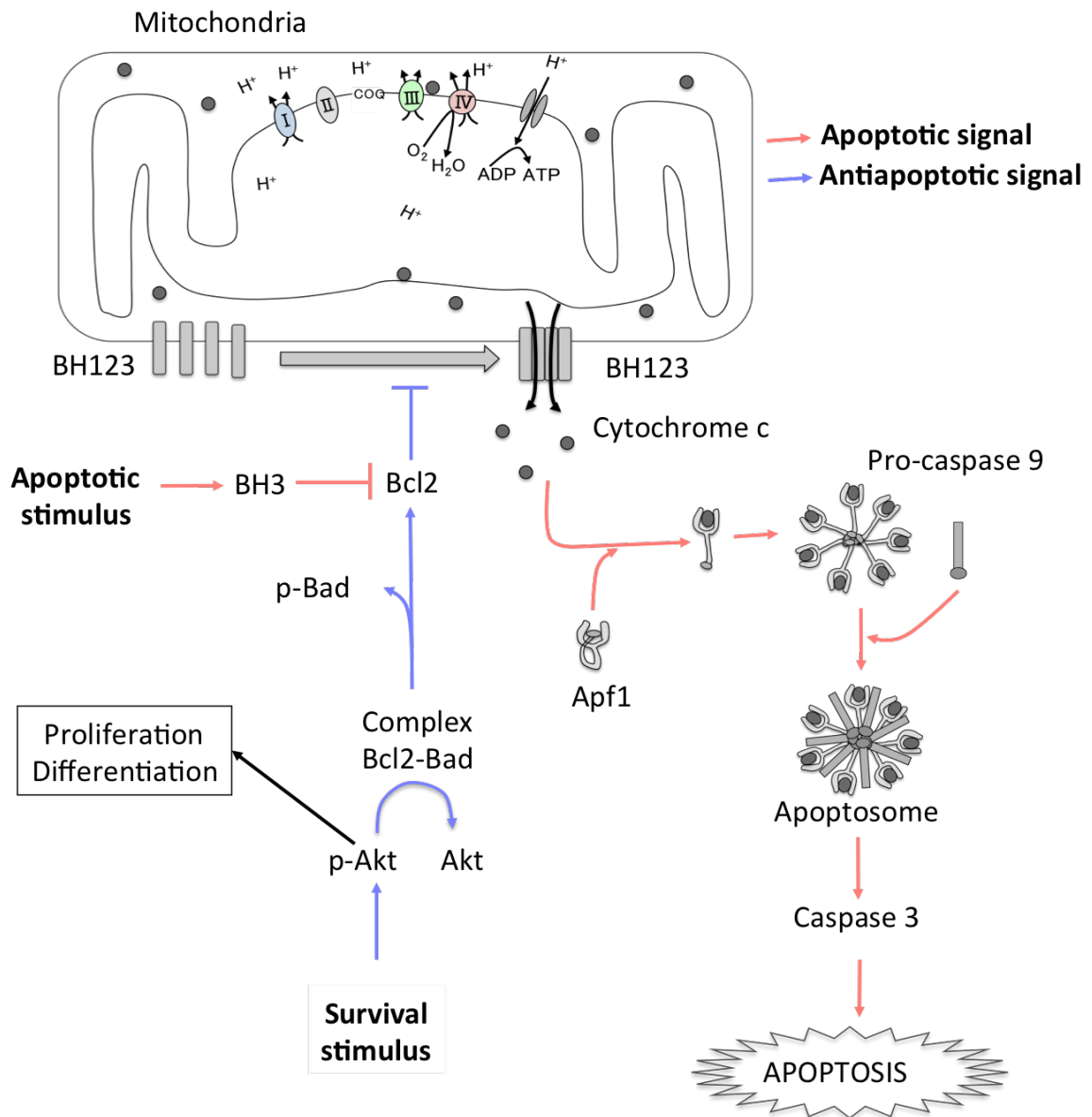


Fig. 3 Apoptosis signalling cascade via mitochondria. The Red arrow is apoptosis signal, and blue arrow is Antiapoptosis signal. Mitochondria inner membrane have protein of complex I–V.(Modified from Alberts et al., Molecular Biology of THE CELL, Fifth Edition, Chapter 18)

1.5 Cell types for experiment of LLI

In this thesis, two types of cells were examined as a subject of 532 nm LLI experiment. First experiment is using the human Glioblastoma A-172 cell line (Chapter 2 and 3). This A-172 cells were provided from Dr. Yamanoha's laboratory and started as a collaboration study. Since A-172 cells are cancer cells, the original plan was started to treat the tumor by LLI. Result of 808 nm LLI and 405 nm LLI were reported previously^{45, 46}. The 808 nm LLI delayed cell cycle and suppressed cell proliferation⁴⁵, and the 405 nm LLI promoted the cell death in A-172 cells⁴⁶. This thesis described the experiment of survival rate by using 532 nm LLI and tried to find the efficiency of 532 nm LLI.

Second experiment is using the neural stem/progenitor cells (NSPCs). Neural stem cells have self-renewal ability and multipotency for neurons, astrocytes and oligodendrocytes. Neural progenitor cells have migrating ability to differentiate into neurons. NSPCs can be cultured from mouse embryonic brain using free-floating aggregates (neurosphere's methods). But neural stem cells and neural progenitor cells are difficult to technically separate. And the discrimination of these cell type by immuno-marker remains controversial yet. Thus, we will use the word of NSPCs through this thesis. An *in vitro* experiment using cultured NSPCs was shown in Chapter 4. An *in vivo* experiment was executed using NSPCs induced by mild ischemia condition (Chapter 5).

As mentioned above in this chapter, the effects of LLI are different on various cell types. Thus, the properties of cells are important to consider when the LLI effect is concerned.

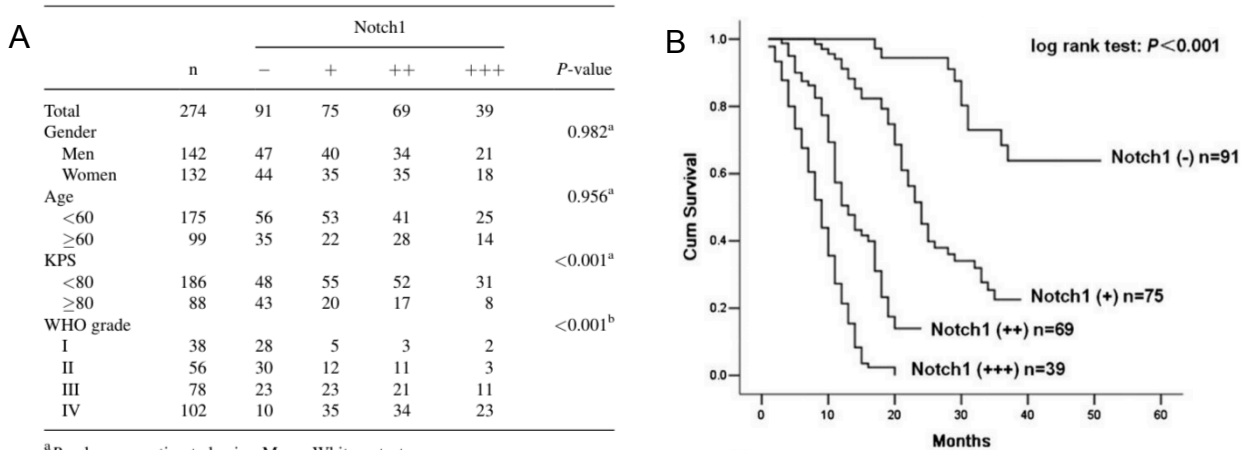
1.5.1 Glioblastoma A-172 cells

The brain tumors are classified from Grade I to IV by World Health Organization (WHO). Grade I gliomas are the least aggressive: subependymal giant cell astrocytoma and pilocytic astrocytoma. Grade II gliomas grow slowly and spread into near normal tissue: pilomyxoid astrocytoma, diffuse astrocytoma and pleomorphic xanthoastrocytoma. Grade III gliomas tend to recur : anaplastic astrocytoma. The highest-grade gliomas (grade IV) maintain rapid growth: glioblastoma, giant cell glioblastoma and gliosarcoma. The survival time of patients with glioblastoma is less than 1 year⁴⁷.

WHO grade of glioma is closely associated with expression of Notch 1, transmembrane protein⁴⁸. Notch 1 expression increased from Grade I to IV based on the hierarchical scores of the immunohistochemical staining (Fig. 4A). This result was not related to patient sex or age. In addition, the survival curve by Kaplan–Meier methods after surgical operation showed relation between survival rate of patients and Notch 1 expression (Fig. 4B).

With regard to discovery of Notch, Thomas Hunt Morgan, an American geneticist, and his colleagues found the fly wings notch or indentation in mutant *Drosophila* in 1913 (Fig. 4C). The fly gene was identified as “Notch” by their additional research in 1917. The relation between Notch and neuron are reported in 1937, and Notch regulated the neurogenic region to determine the cell fate in the development of *Drosophila* embryo in 1937⁴⁹. Furthermore, Greg Lemke and colleagues showed Notch was expressed not only in *drosophila* but also in mammals in 1991. The high amount of Notch expressed between embryonic day 12 and 14 in rat brain, and Notch expression decreased to lower amount in the adult immediately⁵⁰. Recently, it has been reported that Notch signaling maintained neural stem cell in the embryonic telencephalon (forebrain) and adult subventricular zone⁵¹.

Notch signaling cascade is activated by cleavage of intracellular domain from membrane. The cleavage is induced by tumour-necrosis factor α converting enzyme/metalloproteinase (TACE) and the γ -secretase (GS) called presenilin (PS). The liberated intracellular notch (ICN) enters the nucleus and prompts the transcription (Fig. 4D)⁵². It is well known that GS-mediated intracellular processes activate Notch signaling pathway, which is associated with cell proliferation and differentiation⁵³⁻⁵⁴.



^aP-value was estimated using Mann-Whitney test.

^bP-value was estimated using Kruskal-Wallis test.

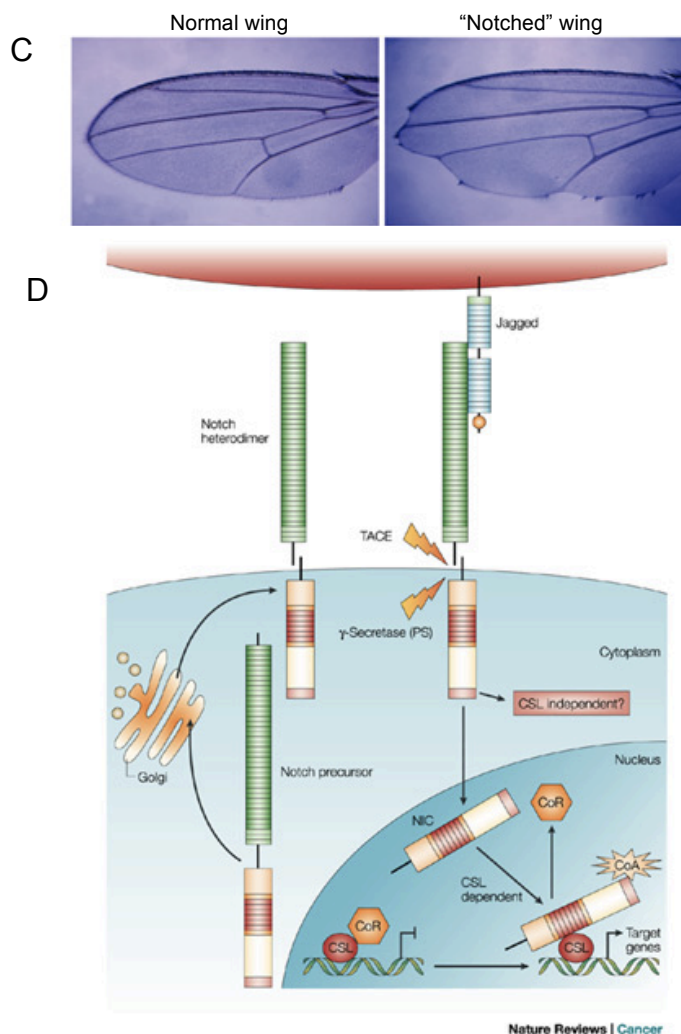


Fig. 4 (A) Notch 1 expression increased from grade I to IV of glioblastoma in human. (From Li J, Cui Y, et al., *J Surg Oncol.* 103(8):813–7, 2011.) (B) Kaplan–Meier postoperative survival curve for patterns of patients with glioblastoma and Notch1 expression. (From Li J, Cui Y, et al., *J Surg Oncol.* 103(8):813–7, 2011.) (C) Left is normal wing in wild type *Drosophila*. Right is “Notched” wing in mutant *Drosophila*. (from POULSON D. F., *PNAS.* 23, 133–137. 1937) (D) Notch signaling cascade is activated by γ -secretase. The intracellular notch (ICN) domain moves to nucleus. (From Freddy Radtke et al., *Nature Reviews Cancer* 3, 756–767, 2003)

1.5.2 Effect of γ -secretase inhibitor (GSI) on Notch and APP

The γ -secretase inhibitor (GSI) can inhibit Notch signaling, which prevent the proliferation of cancer cells. There are GSI isotypes with more than 100, and the types are classified into 2: transition state analog and non-transition state analog. The transition state analog, which binds to active GS, is known the IL X (cbz-IL-CHO). It decreases the expression of as a transcription factor HES-1, and arrest the G0-G1 cell cycle in the human tongue carcinoma Tca8113 cell⁵⁵). The non-transition state analogs, which binds to the non-active site and interfere the GS, one of them is known as N-[N-(3,5-difluorophenacetyl)-L-alanyl]-S-phenylglycine t-butyl ester (DAPT)⁵⁶), a dipeptide inhibitor of the benzodiazepine type (Fig. 5). The DAPT decrease the cell proliferation and arrest the cell cycle using culture of glioblastoma cell line U87MG, U251MG, T98G, and A-172 *in vitro* ⁵⁷).

GSI:DAPT

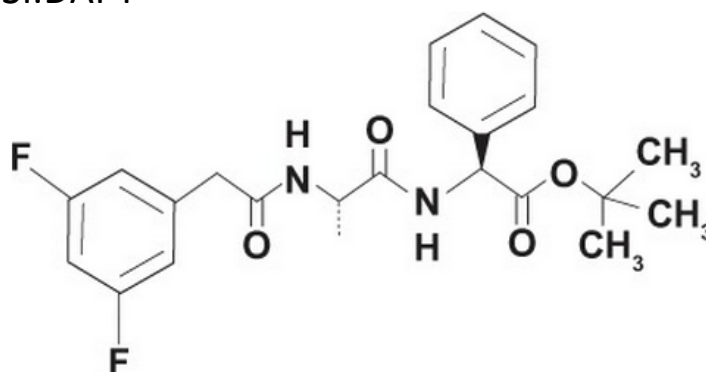


Fig. 5. Structure of DAPT.

While GSI has been investigated to treat the cancer, it was also examined to prevent the progress of the Alzheimer's disease (AD). The number of AD patients will almost double every 20 years, reaching 65.7 million in 2030 and 115.4 million in 2050⁵⁸). In the Alzheimer's disease, the brain is atrophied, has a reduced brain weight and has enlarged ventricles. Gradually the

basic ability for memory, language, calculation, and visuospatial perception is lost along progressing the brain abnormality. The surface of the brains in AD patients observed the amyloid plaques, large aggregates of filament protein. The amyloid plaques are consisted of small peptides named Amyloid beta (A β). A β is considered as a pathogenic agent of Alzheimer's disease that is processed from amyloid precursor protein (APP) by GS⁵⁹). Intracellular, as well as extracellular, accumulations of A β result in nerve cell toxicity⁶⁰). As GS activity is essential for the release of intact A β , GSIs have been contemplated for the treatment of Alzheimer's disease.

Since GSIs have been shown to decrease A β production after administration to transgenic mice overexpressing human APP⁶¹), they were considered as useful drugs to lower A β accumulation for long-term treatment in human patients⁶²). Despite of the potential benefit, GSIs could have side effects. For example the mice suppressed APP expression (APP Knockout mice) increased spine density in the cerebral cortex, and DAPT induced reduction of the dendritic spines⁶³). In addition, GSI side effects related to cell survival via Notch signaling. It is well known that GS-mediated intracellular processes activate Notch signaling pathway as mentioned above. Notch regulates the expression of a phosphatase PTEN (Phosphatase and Tensin homolog deleted from chromosome) via ICN, the intracellular moiety of Notch. When ICN is released from Notch by GS, ICN bind to the transcriptional targets including MYC and HES1. HES1 suppresses the expression of PTEN, which dephosphorylates a phosphoinositide that is critical for activation of Akt⁶⁴) (Fig. 6). Activated Akt plays key roles not only in mediating antiapoptotic cell survival as mentioned in subsectional above but also cell proliferation, cell-cycle progression, differentiation, transcription, translation, and glucose metabolism⁶⁵).

Therefore, although GSIs could be effective for treating Alzheimer's disease with their inhibitory role of A β expression and accumulation, they have unwanted side effects of suppressing cell proliferation and survival by inhibiting Akt activation via PTEN elevation. These dual aspects of GSIs await other novel drugs or treatments that ameliorate the side effects.

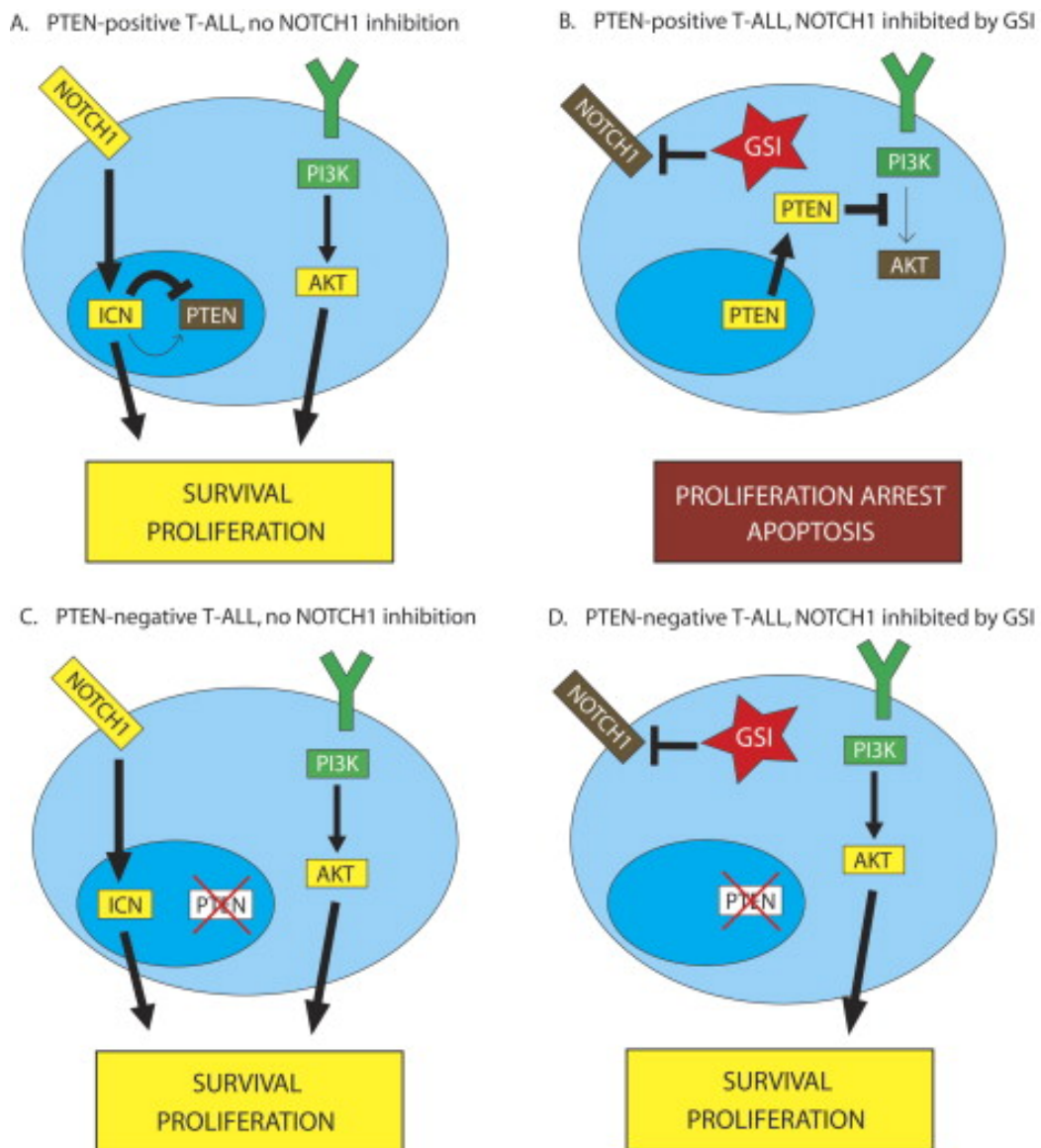


Fig. 6 The suppressed PTEN leads to resistance to inhibition of NOTCH1 but dependence on Akt Signaling. (From Gutierrez A et al. *Cancer Cell* 12: 411–413., 2007.)

(A) Low expression of PTEN cannot inhibit the PI3K-Akt pathway.

(B) γ -secretase inhibitors (GSIs) blocks ICN. And, the HES1-mediated inhibition of PTEN expression is relieved, and PTEN can therefore inhibit the Akt activation.

(C and D) In the mutant of PTEN, uninhibited Akt activation leads to aberrant survival and proliferation independent of NOTCH1 pathway activity

1.5.3 Embryonic neural stem/progenitor cells (NSPCs)

Cortical neurons are classified into two major cell types, the excitatory pyramidal glutamatergic neurons (80%) and the inhibitory GABAergic neurons (20%)⁶⁶. The pyramidal neurons provide the structural inputs and outputs of the cortex and separate cortical layer from layer 1 to 6 by characteristic axonal connections, dendritic morphologies and physiological properties. The pyramidal neurons in the deep layers (layer 5/6) projects to subcortical structures including thalamus, basal ganglia, and spinal cord. Besides, the neurons in upper layer (layer 2/3) projects intra-cortically to other cortical areas⁶⁶. Inhibitory GABAergic neurons regulate cortical function through local connections.

During development, glutamatergic neurons and GABAergic neuron in the cortex are generated in different locations. Glutamatergic neurons are born in the ventricular zone (VZ) and subventricular zones (SVZ) of embryonic cortex in dorsal telencephalon. After exited the cell cycle, glutamatergic cells migrate to the cortical plate (CP) along the radial glia cells (RG)⁶⁷ (Fig. 7). GABAergic neurons are born in the ganglionic eminence (GE) in ventral telencephalon. NSPCs localized in the medial GE (MGE) and caudal GE (CGE), and preoptic area (POA) give rise to cortical GABAergic interneurons, whereas lateral (LGE) NSPCs produce GABAergic cell populations of olfactory bulb (OB), amygdala, and striatum. GABAergic neurons migrate tangentially from GE into the cortex through the marginal zone (MZ) and the subventricular/intermediate zones (SVZ/IZ) firstly and then radially migrate to the CP of their final laminar position (radial migration). 3% of GABAergic neurons arrive in the MZ or SVZ/IZ from GE at E13.5 mouse (Fig.8A, 8J, 8A'). By the next day (E14.5), most of GABAergic neurons to stay in the cortex exist in the MZ or SVZ/IZ, but only ~20% GABAergic cells enter into CP at this age (Fig.8B, 8J, 8B'). This proportion of GABAergic cell in CP is maintained during cortical development until after P7⁶⁸ (Fig. 8C–I, 8J, 8C'–8I').

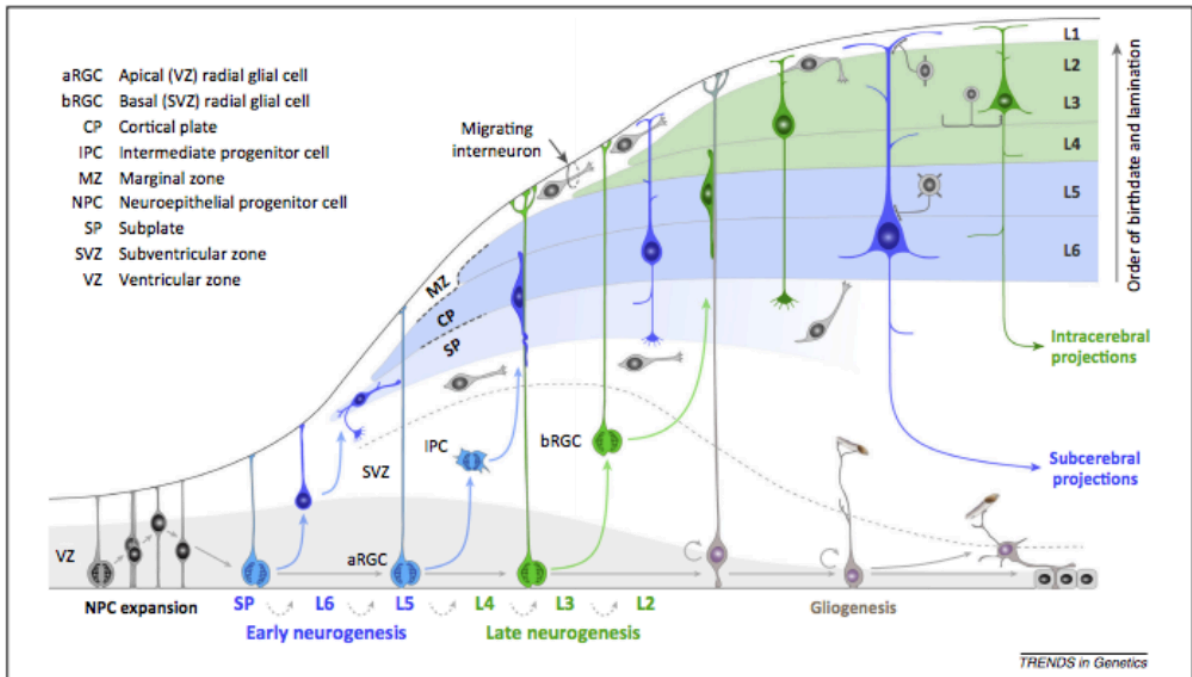


Fig. 7 Glutamatergic neuron migrate into cortical plate (CP) after generated at ventricular zone (VZ) and subventricular zones (SVZ). (From Shibata M, et al., Trends Genet. 2:77–87, 2015.)

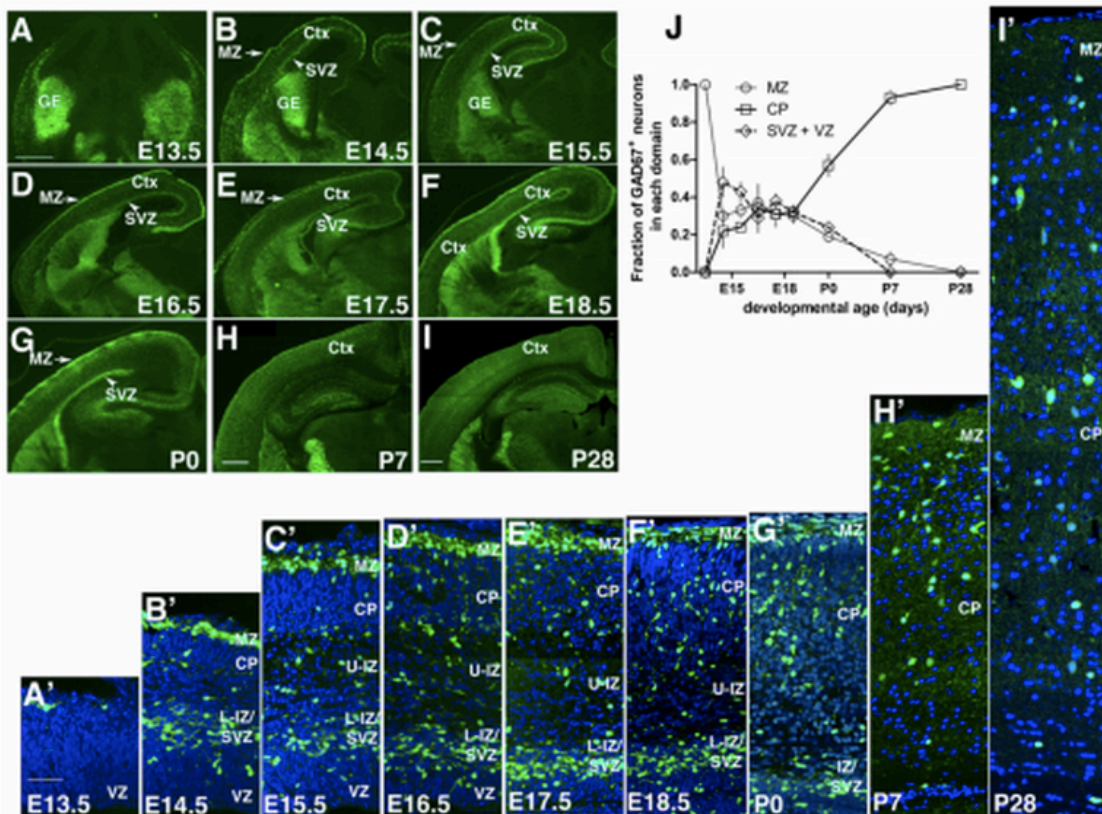


Fig. 8 GABAergic neuron (Green) born in Ganglionic Eminence at dorsal region. The cells tangentially migrate upper layer (Marginal Zone:MZ) and deep layer (SVZ/IZ) of CP at the first. Depend on the development of cortical layer, the GABAergic cells radially migrate to CP. (From Sahara S, et al., J Neurosci., 32–14:4755–61., 2012.)

1.5.4 Adult NSPCs

One century ago, Santiago Ramon y Cajal (1852-1934) mentioned: “Once development was ended, the fonts of growth and regeneration of the axons and dendrites dried up irrevocably. In adult centers, the nerve paths are something fixed and immutable: everything may die, nothing may be regenerated. It is for the science of the future to change, if possible, this harsh decree”. This Cajal’s dogma was believed until the early 1990s among the community of neuroscientists and medical workers.

Adult neurogenesis was discovered in rodent hippocampus and olfactory bulb with experiments of [³H]-thymidine autoradiography by Joseph Altman in 1960s. However it was not accepted widely for a few decades. Furthermore, Fernando Nottebohm showed adult neurogenesis birds learned singing in the 1980s. Unfortunately, due to the dogma in adult neurogenesis, these findings were ignored in the field of neuroscience. These articles saw the light of the day after the development of novel methods for labeling newly generated cells such as BrdU, immunohistochemical marker and retrovirus. Now it is well accepted that NSPCs exist in the two areas of the brain, the dentate gyrus (DG) of the hippocampus and the subventricular zone (SVZ), whose projection through the rostral migratory stream to the olfactory bulb⁶⁹(Fig.9).

In addition to DG and SVZ, it was reported that NSPCs exist in layer 1 of adult mammalian cortex⁷⁰. NSPCs in layer 1 produced GABAergic neurons by mild ischemia surgery. Ohira et al. injected retrovirus vector into layer 1 and white matter. Then the brain sections were stained with GABAergic neuron marker (GAD67) and Cell cycle marker (Ki67). Triple positive cells (Ki67, GAD67 and GFP) meaning proliferating GABAergic neuron were found in and beneath layer 1. Ischemia treatment increased not only the number of the cells but also GAD67 and GFP positive with Ki67-negative cells meaning exist cell cycle after proliferation in layers 2–6, which are supposedly NSPCs in layer 1 exited from cell cycle and migrated from layer 1 to layers below. They injected retrovirus vector into the white matter on the mild ischemia condition, but few newly generated neurons were found in cortex. The NSPCs might be derived from GE because they were stained with Nkx2.1 and MafB, which are GE markers.

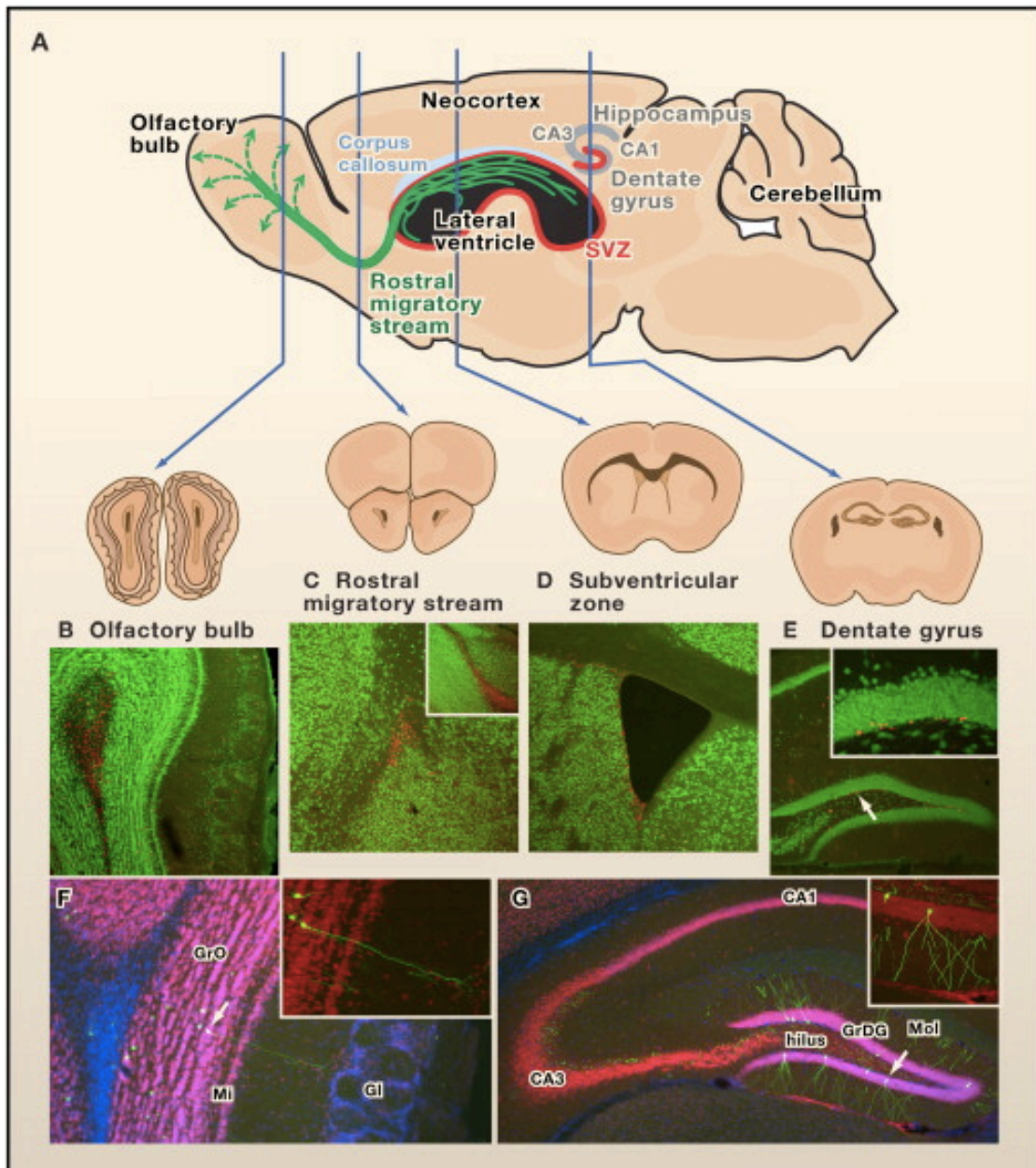


Fig. 9 (A) The Neurogenesis area in the adult mouse brain. Red: the subgranular zone (SGZ) of the dentate gyrus (DG) in the hippocampus and the subventricular zone (SVZ) of the lateral ventricles. (B–E) BrdU (red) and NeuN (green) staining (B) Olfactory bulb, (C) Rostral migratory stream, (D)SVZ, and (E)DG. (F and G) Newborn neurons labeled by retrovirus-mediated expression of green fluorescent protein (GFP). The arrows are high-magnification red, NeuN(Red), GFP(green), DAPI(blue). (FH.Gage et al, Cell., 22;132(4):645–60., 2008)

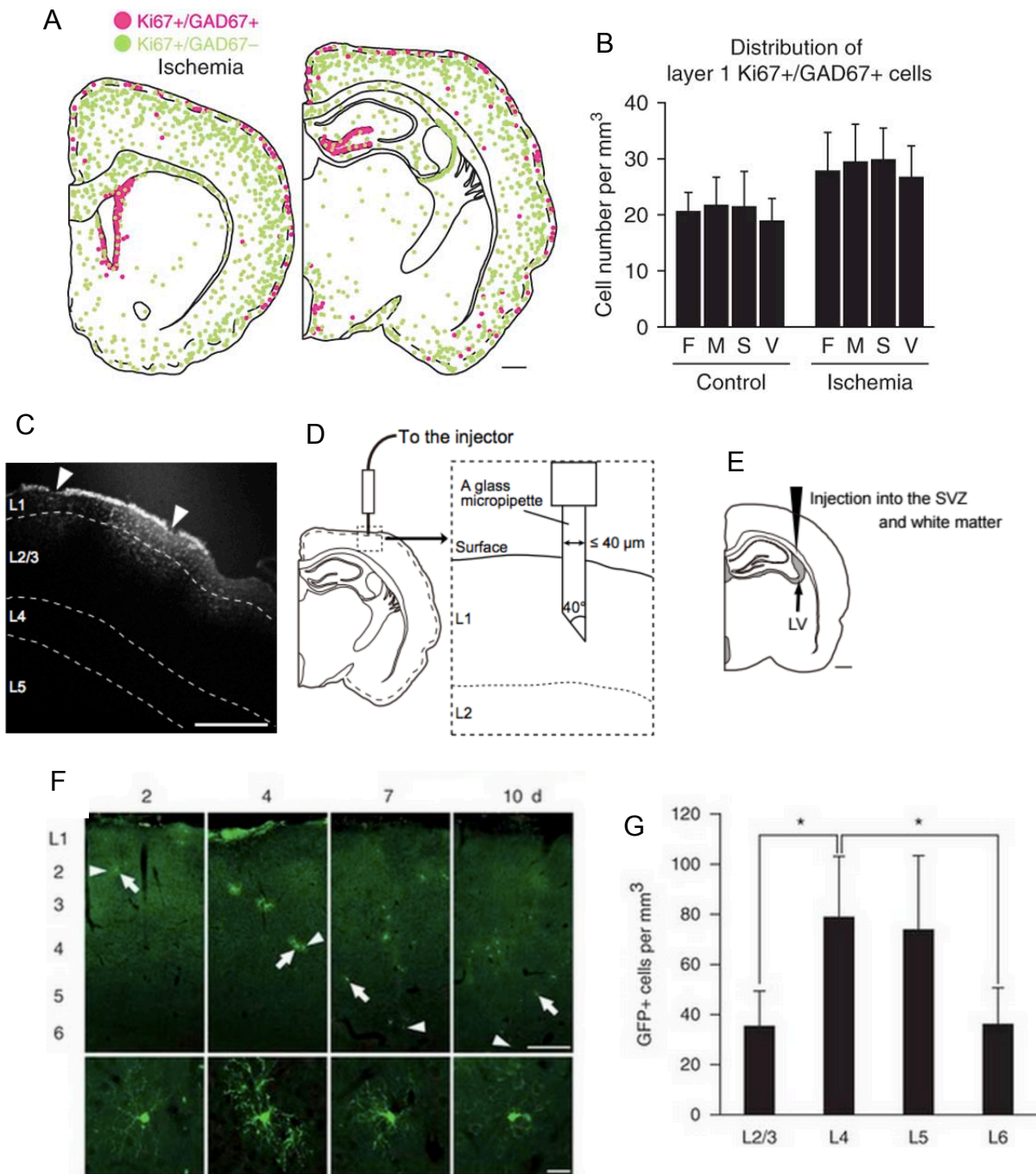


Fig.10 The neurogenesis in layer 1 of adult rat brain. (A, B) Distribution of Ki67 and Gad67 positive cells in the ischemic rat brains. (C) A diffuse of the injected solution of a Hoechst 33258 was limited at layer 1. Arrowheads: injection sites. Scale bar: 500 μm. (D) Schematic of the injection in layer 1 and (E) white matter of somatosensory cortex. (E) Time course of the newborn neurons labeled by retrovirus-mediated expression of green fluorescent protein (GFP). (F) Laminar distribution of GFP+ cells at 4 weeks after mild ischemia (*P < 0.05, two-way ANOVA followed by Tukey's post hoc test.). (Ohira et al., Nat. Neurosci., 13(2):173–9., 2010)

1.6 References

- 1) Richard P. (2014) Feynman with a new introduction by A. Zee., QED: The Strange Theory of Light and Matter., eBook ISBN: 9781400847464.
- 2) Kalloniatis M, Luu C.,(1995) The Perception of Color., The Organization of the Retina and Visual System. Salt Lake City (UT): University of Utah Health Sciences Center.
- 3) Jan Frercks, Heiko Weber, Gerhard Wiesenfeldt.(2009) Reception and discovery: the nature of Johann Wilhelm Ritter's invisible rays., Studies in History and Philosophy of Science, 40, 143–156.
- 4) Bernstein C, Bernstein H, Payne CM, Garewal H.(2002) DNA repair/pro-apoptotic dual-role proteins in five major DNA repair pathways: fail-safe protection against carcinogenesis., Mutat Res. 11(2):145–78.
- 5) Lucock M, Jones P, Martin C, Beckett E, Yates Z, Furst J, Veysey M.(2015) Vitamin D: Beyond Metabolism., J Evid Based Complementary Altern Med. pii: 2156587215580491.
- 6) Gould, R. Gordon (1959). "The LASER, Light Amplification by Stimulated Emission of Radiation". *The Ann Arbor Conference on Optical Pumping*, p.128.
- 7) Jan Tunér (2010) LASER DENTISTRY/LOW LEVEL LASER THERAPY: Therapeutic lasers expand the scope of dentistry., Bio optics world. <http://www.bioopticsworld.com/articles/print/volume-3/issue-5/features/laser-dentistry-low-level-laser-therapy-therapeutic-lasers-expand-the-scope-of-dentistry.html>
- 8) Beard P (2011) Biomedical photoacoustic imaging, *Interface Focus*.1(4):602–31.
- 9) Te AE (2006) The Next Generation in Laser Treatments and the Role of the GreenLight High-Performance System Laser. *Rev Urol*. 8, 3:24–30.
- 10) Rojas JC, Gonzalez-Lima F (2011) Low-level light therapy of the eye and brain. *Eye and Brain* 3, 49–67.
- 11) Karu T (1989) Photobiology of low-power laser effect, *Health Physics*. 56: 691–704.
- 12) da Silva JP, da Silva MA, Almeida AP, Lombardi Junior I, Matos AP (2010) Laser therapy in the tissue repair process: a literature review. *Photomed Laser Surg* 28: 17–21.
- 13) Brosseau L, Robinson V, Wells G, Debie R, Gam A, et al. (2005) Low level laser therapy (Classes I, II and III) for treating rheumatoid arthritis. *Cochrane Database Syst Rev*.

4:CD002049.

- 14) Bjordal JM, Lopes-Martins RA, Joensen J, Couppe C, Ljunggren AE, et al. (2008) A systematic review with procedural assessments and meta-analysis of low level laser therapy in lateral elbow tendinopathy (tennis elbow). *BMC M Disorders*
- 15) Jamtvedt G, Dahm KT, Christie A, Moe RH, Haavardsholm E, et al. (2007) Physical therapy interventions for patients with osteoarthritis of the knee: an overview of systematic reviews. *Phys Ther* 88: 123–136. doi: 10.2522/ptj.20070043
- 16) Oron A, Oron U, Chen J, Eilam A, Zhang C, et al. (2006) Low-level laser therapy applied transcranially to rats after induction of stroke significantly reduces long-term neurological deficits. *Stroke* 37(10):2620–4.
- 17) Lampl Y, Zivin JA, Fisher M, Lew R, Welin L, et al. (2007) Infrared laser therapy for ischemic stroke: a new treatment strategy: results of the NeuroThera Effectiveness and Safety Trial-1 (NEST-1). *Stroke* 38(6):1843–9.
- 18) Zhang Q, Zhou C, Hamblin MR, Wu MX (2014) Low-level laser therapy effectively prevents secondary brain injury induced by immediate early responsive gene X-1 deficiency. *J Cereb Blood Flow Metab* 34:1391–401.
- 19) Esmaeelinejad M, Bayat M, Darbandi H, Bayat M, Mosaffa N.(2014) The effects of low-level laser irradiation on cellular viability and proliferation of human skin fibroblasts cultured in high glucose mediums. *Lasers Med Sci.* 29(1):121–9.
- 20) Jia YL, Guo ZY. (2014) Effect of low power He-Ne laser irradiation on rabbit articular chondrocytes in vitro. *Lasers Surg Med* 34:323–328.
- 21) Stadler I, Evans R, Kolb B, Naim JO, Narayan V, Buehner N, Lanzafame RJ.(2000) In vitro effects of low-level laser irradiation at 660 nm on peripheral blood lymphocytes., *Lasers Surg Med.* 27(3):255–61.
- 22) Moore P, Ridgway TD, Higbee RG, Howard EW, Lucroy MD.(2005)Effect of wavelength on low-intensity laser irradiation-stimulated cell proliferation in vitro., *Lasers Surg Med.* 36(1):8–12.
- 23) Sroka R, Schaffer M, Fuchs C, Pongratz T, Schrader-Reichard U, Busch M, Schaffer PM, Dühmke E, Baumgartner R.(1999) Effects on the mitosis of normal and tumor cells induced by light treatment of different wavelengths., *Lasers Surg Med.* 25(3):263–71.

- 24) Liu YH, Ho CC, Cheng CC, Hsu YH, Lai YS.(2006) Photoradiation could influence the cytoskeleton organization and inhibit the survival of human hepatoma cells in vitro., *Lasers Med Sci.* 21(1):42–8.
- 25) Machneva TV, Protopopov DM, Vladimirov IuA, Osipov AN.(2008) A study of the effect of low-intensity laser radiation of the blue, green, and red spectral regions on the healing of experimental skin wounds in rats, *Biofizika.* 53(5):894–901.
- 26) Kassák P, Przygodzki T, Habodászová D, Bryszewska M, Sikurová L.(2005) Mitochondrial alterations induced by 532 nm laser irradiation. *Gen Physiol Biophys* 24: 209–220.
- 27) Gresner P, Watała C, Sikurová L.(2005) The effect of green laser light irradiation on whole blood platelets. *J Photochem Photobiol B* 79: 43–50.
- 28) Anwer AG1, Gosnell ME, Perinchery SM, Inglis DW, Goldys EM.(2012) Visible 532 nm laser irradiation of human adipose tissue-derived stem cells: effect on proliferation rates, mitochondria membrane potential and autofluorescence. *Lasers Surg Med* 44(9):769–78.
- 29) Karu T (2003) *Low Power Laser Therapy.* Biomedical Photonics Handbook 48: CRC Press. 48 p.
- 30) Gao X, Xing D (2009) Molecular mechanisms of cell proliferation induced by low power laser irradiation. *J Biomed Sci.* 16:4. doi: 10.1186/1423-0127-16-4.
- 31) McBride HM, Neuspiel M, Wasiak S (2006) Mitochondria: more than just a powerhouse. *Curr Biol* 16: 551–560.
- 32) Mochizuki-Oda N, Kataoka Y, Cui Y, Yamada H, Heya M, Awazu K.(2002)Effects of near-infra-red laser irradiation on adenosine triphosphate and adenosine diphosphate contents of rat brain tissue., *Neurosci Lett.*,323(3):207–10.
- 33) Sharma SK, Kharkwal GB, Sajo M, Huang YY, De Taboada L, McCarthy T, Hamblin MR.(2011) Dose response effects of 810 nm laser light on mouse primary cortical neurons., *Lasers Surg Med.*, 43(8):851–9.
- 34) Karu T, Pyatibrat L, Kalendo G.(2001) Studies into the action specifics of a pulsed GaAlAs Laser ($\lambda=820$ nm) on a cell culture., *Lasers in the Life Sciences* (9):203–210.
- 35) Karu T, Pyatibrat L, Kalendo G.(1995) Irradiation with He-Ne laser increases ATP level in cells cultivated in vitro., *J Photochem Photobiol B.*, 27(3):219–23.
- 36) Kim D, Chung J (2002) Akt: Versatile Mediator of Cell Survival and Beyond. *Journal of*

Biochemistry and Molecular Biology 35: 106–115.

- 37) Zhang L, Xing D, Gao X, Wu S (2009) Low-power laser irradiation promotes cell proliferation by activating PI3K/Akt pathway. *J Cell Physiol* 219: 553–562.
- 38) Shefer G, Partridge TA, Heslop L, Gross JG, Oron U, et al. (2002) Low-energy laser irradiation promotes the survival and cell cycle entry of skeletal muscle satellite cells. *J Cell Sci* 115: 1461–1469.
- 39) Azevedo LH, de Paula Eduardo F, Moreira MS, de Paula Eduardo C, Marques MM (2006) Influence of different power densities of LILT on cultured human fibroblast growth. *Lasers Med Sci*, DOI 10.1007/s10103-006-0379-9.
- 40) Bijur GN, Jope RS (2003) Rapid accumulation of Akt in mitochondria following phosphatidylinositol 3-kinase activation. *J Neurochem* 87: 1427–1435.
- 41) Miyamoto S, Murphy AN, Brown JH (2008) Akt mediates mitochondrial protection in cardiomyocytes through phosphorylation of mitochondrial hexokinase-II. *Cell Death Differ* 15: 521–529.
- 42) Su CC, Yang JY (2012) Mitochondrial Akt-regulated mitochondrial apoptosis signaling in cardiac muscle cells. *Am J Physiol Heart Circ Physiol* 302: 716–23.
- 43) Liang J, Liu L, Xing D (2012) Photobiomodulation by low-power laser irradiation attenuates Ab-induced cell apoptosis through the Akt/GSK3 β /catenin pathway. *Free Radic Biol Med* 53(7): 1459–1467.
- 44) Palomero T, Sulis ML, Cortina M, Real PJ, Barnes K, et al. (2007) Mutational loss of PTEN induces resistance to NOTCH1 inhibition in T-cell leukemia. *Nature Med* 13: 1203–1210.
- 45) Murayama H, Sadakane K, Yamanoha B, Kogure S (2012) Low-power 808-nm laser irradiation inhibits cell proliferation of a human-derived glioblastoma cell line in vitro. *Lasers Med Sci* 27: 87–93.
- 46) Ang FY, Fukuzaki Y, Yamanoha B, Kogure S (2012) Immunocytochemical studies on the effect of 405-nm low-power laser irradiation on human-derived A-172 glioblastoma cell. *Lasers Med Sci* 27: 935–942.
- 47) International Classification of Diseases for Oncology. http://apps.who.int/iris/bitstream/10665/96612/1/9789241548496_eng.pdf?ua=1
- 48) Li J, Cui Y, Gao G, Zhao Z, Zhang H, Wang X. (2011) Notch1 is an independent prognostic

- factor for patients with glioma. *J Surg Oncol.* 103(8):813–7.
- 49) POULSON, D. F. (1937) Chromosomal deficiencies and the embryonic development of *Drosophila melanogaster*. *Proc. Natl. Acad. Sci. U.S.A.* 23, 133–137.
- 50) Weinmaster G, Roberts VJ, Lemke G.(1991) A homolog of *Drosophila* Notch expressed during mammalian development., *Development.* 13(1):199–205.
- 51) Imayoshi I, Sakamoto M, Yamaguchi M, Mori K, Kageyama R.(2010) Essential roles of Notch signaling in maintenance of neural stem cells in developing and adult brains. *J Neurosci.*, 30(9):3489–98.
- 52) Freddy Radtke & Kenneth Raj.(2003) The role of Notch in tumorigenesis: oncogene or tumour suppressor? *Nature Reviews Cancer* 3, 756–767.
- 53) De Strooper B, Annaert W, Cupers P, Saftig P, Craessaerts K, et al. (1999) A presenilin-1-dependent γ -secretase-like protease mediates release of Notch intracellular domain. *Nature* 398: 518–522.
- 54) Artavanis-Tsakonas S, Rand MD, Lake RJ (1999) Notch signaling: cell fate control and signal integration in development. *Science* 284: 770–776.
- 55) Yao J, Duan L, Fan M, Wu X.(2007) γ -secretase inhibitors exerts antitumor activity via down-regulation of Notch and Nuclear factor kappa B in human tongue carcinoma cells. *Oral Dis.* 13(6):555–563.
- 56) Purow B.(2012) Notch inhibition as a promising new approach to cancer therapy. *Adv Exp Med Biol.*, 727:305–319.
- 57) Floyd DH, Kefas B, Seleverstov O, Mykhaylyk O, Dominguez C, Comeau L, Plank C, Purow B., *Neuro Oncol.*(2012) Alpha-secretase inhibition reduces human glioblastoma stem cell growth in vitro and in vivo by inhibiting Notch.,14(10):1215–26.
- 58) Prince M, Jackson J (2009) Alzheimer’s Disease International World Alzheimer Report. Global Action on Aging site. Available: <http://www.globalaging.org/health/world/2009/alzheimer.pdf>.
- 59) Li M, Chen L, Lee DH, Yu LC, Zhang Y (2007) The role of intracellular amyloid b in Alzheimer’s disease. *Progress in Neurobiology* 83: 131–139.
- 60) Zhao H, Zhu J, Cui K, Xu X, O’Brien M, et al.(2009) Bioluminescence imaging reveals inhibition of tumor cell proliferation by Alzheimer’s amyloid b protein. *Cancer Cell Int* 1:

9–15.

- 61) Dovey HF, John V, Anderson JP, Chen LZ, de Saint Andrieu P, et al. (2001) Functional c-secretase inhibitors reduce beta-amyloid peptide levels in brain. *J Neurochem* 76: 173–181.
- 62) Dovey HF, John V, Anderson JP, Chen LZ, de Saint Andrieu P, et al. (2001) Functional gamma-secretase inhibitors reduce beta-amyloid peptide levels in brain. *J Neurochem* 76: 173–81.
- 63) Bittner T, Fuhrmann M, Burgold S, Jung CK, Volbracht C, Steiner H, Mitteregger G, Kretzschmar HA, Haass C, Herms J. (2009) Gamma-secretase inhibition reduces spine density in vivo via an amyloid precursor protein-dependent pathway. *J Neurosci.* 29(33):10405–9.
- 64) Conlon RA, Reaume AG, Rossant J (1995) Notch1 is required for the coordinate segmentation of somites. *Development* 121: 1533–1545.
- 65) Gutierrez A, Look AT (2007) Notch and PI3K-Akt Pathways Intertwined. *Cancer Cell* 12: 411–413.
- 66) Eric R. Kandel, James H. Schwartz, Thomas M. Jessell, Steven A. Siegelbaum, A.J. Hudspeth. *Principles of neural science*, fifth edition, Part IV p348.
- 67) Shibata M, Gulden FO, Sestan N. (2015) From trans to cis: transcriptional regulatory networks in neocortical development. *Trends Genet.* 2:77–87.
- 68) Sahara S, Yanagawa Y, O'Leary DD, Stevens CF. (2012) The fraction of cortical GABAergic neurons is constant from near the start of cortical neurogenesis to adulthood. *J Neurosci.* 4;32(14):4755–61.
- 69) Zhao C, Deng W, Gage FH. (2008) Mechanisms and functional implications of adult neurogenesis. *Cell.* 22;132(4):645–60.
- 70) Ohira K, Furuta T, Hioki H, Nakamura KC, Kuramoto E, Tanaka Y, Funatsu N, Shimizu K, Oishi T, Hayashi M, Miyakawa T, Kaneko T, Nakamura S. (2010) Ischemia-induced neurogenesis of neocortical layer 1 progenitor cells. *Nat. Neurosci.* 13(2):173–9.

Chapter 2

Effect of 532 nm LLI on proliferation of glioblastoma A-172

Contents

2.1 Introduction

2.2 Materials and Methods

2.2.1 Cell culture of glioblastoma (A-172)

2.2.2 Laser irradiation method

2.2.3 Cell counting by microscopic observations

2.2.4 Cell Viability by MTT Assay

2.2.5 Analysis of ATP level in cell lysate

2.2.6 Statistical analysis

2.3 Results

2.2.1 Effects of 532 nm LLI on the number of A-172 cells

2.2.2 ATP level in cell lysates

2.4 Discussion

2.5 References

2.1 Introduction

In our previous study, we used human-derived glioblastoma A-172 cells which is brain cancer cells. Results showed that 808 nm LLI delayed cell cycle⁷¹⁾ and 405 nm LLI promoted cell death⁷²⁾. Thus we investigated how 532 nm LLI effect on proliferation of glioblastoma A-172 cells. In addition, ATP level in A-172 after LLI were examined.

2.2 Materials and Methods

2.2.1 Cell culture of glioblastoma (A-172)

The human-derived glioblastoma A-172 cell line was obtained from JCRB (#0228). The cells of subculture were cultured in T25-flasks, 25 cm² canted neck and vented cap. Cultured medium was prepared based on DMEM (Dulbecco's Modified Eagle Medium) and added streptomycin, penicillin, HEPES and sodium bicarbonate (Table 2). The medium was pH adjusted to 7.0 (Recommended working pH is 7.0–7.4. Because DMEM will become more alkali while doing filtration, pH7.0 is appropriate). Sterile containers by membrane filtration with 0.22 μm filter using the pump to make a positive pressure. 10% fetal bovine serum (FBS) was added to pre-warmed DMEM medium. The frozen A-172 cells in cryotube were rapidly thawed in 37°C water bath and added to 10 ml 10% FBS-DMEM medium. The medium containing cells were moved into T-25 flasks, and incubated in an atmosphere of 5% CO₂, 95% air at 37°C. Next day, all medium were replaced to remove the dead cells. During the subculture, the medium was changed once every three days to maintain cell growth. Trypsinization was performed using 0.1% trypsin-PBS once the cells reached 80% confluency (10⁶ cells). Cells were plated in 35 mm dish (Sumitomo Bakelite Co. Ltd., Tokyo, Japan), 96-well plates (Sumitomo Bakelite Co. Ltd., Tokyo, Japan), or LAB-TEK Chamber Slide (Nalge Nunc International, New York, USA) with 10% FBS-DMEM medium at 6×10³ cells/ml. To cryopreserve the cells, cells with 10% DMEM, 20% FBS in DMEM medium were added to cryotube and keep into the BICELL (NIHON FREEZER) for 12–16h at -80°C, and stored at the preferential box.

Table 2 The preparation of DMEM medium

Contents	Store	Volume
DMEM (powder)	4°C	6.7 g
Streptomycin	RT	0.050 g
Penicillin	RT	0.015 g
HEPES	RT	1.75 g
NaHCO ₃	RT	1.85 g
ddH ₂ O	RT	450 ml
After adjust pH7.0, add H ₂ O till 500 ml		

2.2.2 Laser irradiation method

The experiment of laser irradiation was conducted in a clean bench. Two hot plates were put in clean bench to heat until 37°C and the hot plates switched on keeping warm to incubate. The CulturePal CO₂ (Cosmobio Co. Tokyo, Japan) and the Gas-tight container were used in order to keep 5% CO₂ during LLI irradiation. Then a preliminary experiments was carried out whether cells are able to culture under this environment or not. The cultured cells put in CulturePal CO₂ which is instrument as a transport for cultured cells. The condition of CulturePal CO₂ under the 37°C at clean bench was compared with CO₂ incubator (normal condition). The cell morphology and proliferation in the CulturePal CO₂ were same as normal condition in CO₂ incubator. A diode laser apparatus (Nd:YVO₄, CW, 532 nm, 0–180 mW) was placed in the clean bench. The laser beam was reflected on a mirror and introduced to cells from the top of the dish. The averaged power was 60 mW measured by power meter, and the irradiated area was 7.1 mm², the calculated power density was 845 mW/cm². In experimental group, the center of dish or well was irradiated for 20, 40 and 60 min with an energy density of 10.1, 20.3, 30.4×10² J/cm², respectively.

2.2.3 Cell counting by microscopic observations

On the day following plating, culture wells on the clean bench maintained at 37°C and in an atmosphere containing 5% CO₂ were photographed with a digital camera before LLI. After taking photographs, the plate was returned to the incubator. Photos were taken immediately after LLI, and 24 and 48 h after LLI. The photos were displayed on a PC monitor and cells were counted per unit area in all areas including the directly irradiated area (Fig. 11).

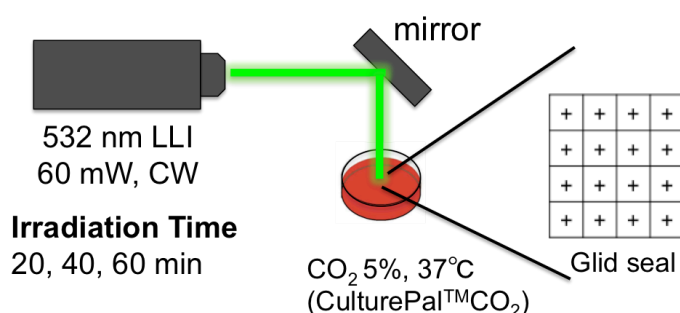


Fig. 11 Schematic diagram of cell counting

2.2.4 Cell viability by MTT Assay

Cell viability was measured by the MTT (3-(4,5-dimethylthiazol-2-yl)-2,5-diphenyl-2H-tetrazolium bromide) colorimetric assay.

The A-172 cells were plated at 0.3×10^4 cells/well in a 96-well plate (200 μ l/well) and incubated for 12 hours. At 48 h after LLI, the culture medium was removed, and 200 μ l of fresh medium containing 20 μ l of MTT (6 mg/ml; Sigma-Aldrich Japan, Tokyo, Japan) was added to each well. The cells were incubated at 37°C for 3 h. Colored precipitates were extracted with 100 μ l of acidic isopropanol at room temperature for 1 h, and the absorbance was measured at 570 nm using a plate reader.

2.2.5 Analysis of ATP level in cell lysate

An ATP/ADP ratio assay kit (EnzyLight™, BioAssay Systems, CA, USA) was used to quantify ATP amount. A-172 cells were plated at 0.5×10^4 cells/well in a 96-well plate (200 μ l/well) and incubated for 12 hours. The culture medium was removed after LLI. 90 μ l ATP reagent was added to each 96-well and mixed by tapping the plate. After 1 min, luminescence (RLU A) was read on a luminometer (ATTO BIO-INSTRUMENT, Tokyo, Japan). 10 minutes after measuring RLU A, the luminescence of samples was read again (RLU B). This measurement provides the background prior to measuring ADP. Immediately following RLU B measurement, 5 μ l ADP reagent was added to each well and mixed by pipetting up and down. After 1 min, luminescence (RLU C) was read for ADP level. The following formula was used to calculate ATP/ADP ratio: $(RLU C - RLU B)/RLU A$.

2.2.6 Statistical analysis

All values were presented as mean \pm SD. Student's two-tailed non-paired t-test and one-way ANOVA were used to analyze statistical differences between 2 groups or among multiple groups, respectively.

2.3 Results

2.3.1 Effects of 532 nm LLI on the number of A-172 cells

We have examined if LLI affects the proliferation of A-172 cells grown in culture. The cells were plated at 0.3×10^4 cells/well in 96-well plates and were irradiated with 532 nm LLI for 0 (no LLI: control), 20, 40, and 60 min. The number of cells remaining at 24 and 48 hours after LLI was counted and compared to that before LLI (Pre-LLI) (Fig. 12). At 24 h after LLI, the proliferation ratio, the number of remaining cells after LLI normalized to that of untreated control, was $110 \pm 14\%$, $111 \pm 16\%$, or $111 \pm 17\%$ for 20 min, 40 min, or 60 min LLI, respectively (Fig. 12B-left bars, no significances among any groups). At 48 h, they were $158 \pm 15\%$ for control, $170 \pm 19\%$, $175 \pm 18\%$, or $180 \pm 12\%$ for 20 min, 40 min, and 60 min LLI, respectively (Fig. 12B, right bars, $n = 12$, $p < 0.05$ for 20 and 40 min LLI, $p < 0.01$ for 60 min LLI).

In addition to cell counts, we also used a calorimetric method to quantify the proliferation and survival in cell culture using the MTT assay. The mean optical density at 570 nm at 48 hours after 40 or 60 min LLI increased significantly over non-irradiated control (Fig. 12C, $n = 16$, $p < 0.01$ for 40 and 60 min LLI), while little change was observed with 20 min LLI.

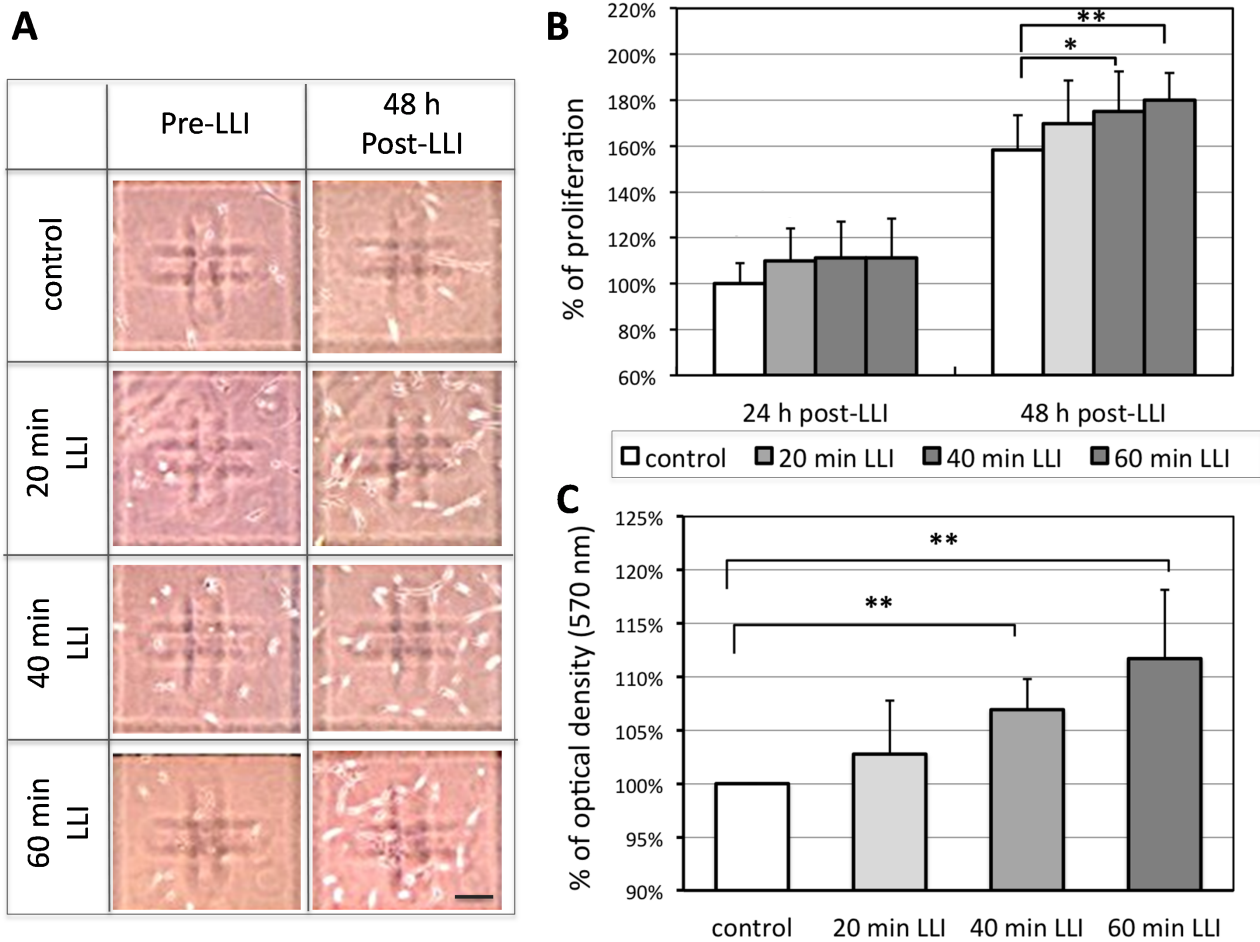


Fig. 12 Effects of LLI on the number of A-172 cells.

A: Sample images of A-172 cells under light microscope. The number of cells increased 48 h post-LLI (right column) after 20, 40, 60 min LLI compared to pre-LLI (left column). Cal.: 100 μ m.

B: Proliferation ratio (the ratio of cell number at 24 or 48 hours following LLI and cell number before LLI) was normalized to control (no LLI) (n = 12 for each group).

C: A summary of colorimetric analysis by MTT staining performed at 48 h after LLI (each group: n = 16). The optical density of each group was normalized to the value of control group (no LLI) at 48 h after initial condition. Asterisks: one-way ANOVA, * p<0.05, ** p<0.01.

2.3.2 ATP Level in Cell Lysates

To test the possibility that LLI-induced cell proliferation involves ATP elevation, we examined ATP level in cell lysates using ATP/ADP ratio assay kit (Fig.13). Mean luminescence after 60 min 405 nm LLI decreased significantly over that of control group ($p < 0.05$, $n = 5$), while little changes were observed for 20 or 40 min 405 nm LLI groups. And mean luminescence after 60 min 532 nm LLI increased significantly over that of control group ($p < 0.05$, $n = 5$), while little changes were observed for 20 or 40 min 532 nm LLI groups. 660 nm LLI did not affect to ATP level in each irradiation time.

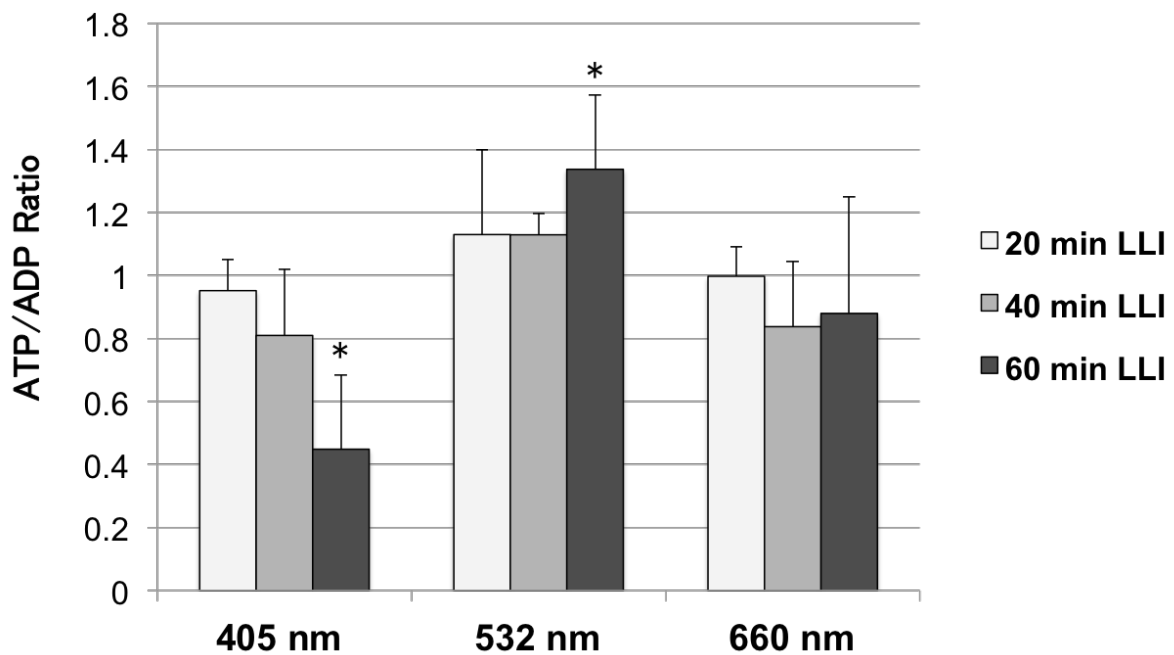


Fig. 13 Effects of LLI on ATP level in cell lysates. The ATP/ADP ratio measured using a luminescence-based assay for control and for 20, 40 and 60 min LLI. The luminescent densities for ATP and ADP were measured 48 h after LLI treatment. The ATP/ADP ratio was calculated and averaged ($n = 5$). Asterisks: one-way ANOVA, * $p < 0.05$.

2.4 Discussion

In the present study, using conventional cell counting and the colorimetric MTT assay, we demonstrate that 532 nm LLI (60 mW) significantly increased viability of human-derived glioblastoma A-172 cells. The effect showed a LLI dose-dependency with 60 min LLI being the most effective for cell proliferation. These findings contrast to studies using LLI of other wavelengths in the same cell type. The infrared 808 nm LLI delayed cell cycle and suppressed cell proliferation⁷¹⁾, and the 405 nm LLI promoted the cell death in A-172 cells⁷²⁾. Thus, the effect of LLI on the cell proliferation appears to depend on the wavelength. Indeed, LLI wavelength-dependent effects were previously reported in various cell types⁷³⁾.

Different effects of LLI wavelength on cell proliferation and survival may depend on photoacceptors present in mitochondria, especially those in the mitochondrial respiratory chain⁷⁴⁾. Primary photoacceptors include cytochromes c oxidase (red and near-infrared light region), NADH-dehydrogenase (blue spectral region), and cytochromes b, c1 and c (green light region). Their cofactors are porphyrins (for cytochrome c oxidase and cytochromes b, c1 and c), or flavins (for NADH-dehydrogenase), respectively⁷⁵⁾. These photoreceptors and cofactors contribute to the generation of ATP, a critical source of chemical energy in cells. Mitochondria are the center of many diverse cellular functions such as signaling, cellular differentiation, cell death, as well as the control of the cell cycle and cell growth⁷⁶⁾. Thus photoacceptors in mitochondria upon light absorption may regulate the level of ATP to support cell survival. However, considering that LLI has different biological effects on different cells, it is difficult to conceive that the regulation of mitochondrial photoacceptors is the only mechanism underlying LLI-mediated cell proliferation. It is likely that final consequences of specific photobiological effects are determined not at the level of primary reactions in the mitochondrial respiratory chain but based on secondary cellular signaling⁷⁴⁾. It will be important to characterize how proteins and enzymes expressed in each cell type contribute to photobiological effects.

2.5 References

- 71) Murayama H, Sadakane K, Yamanoha B, Kogure S (2012) Low-power 808-nm laser irradiation inhibits cell proliferation of a human-derived glioblastoma cell line in vitro. *Lasers Med Sci.* 27: 87–93.
- 72) Ang FY, Fukuzaki Y, Yamanoha B, Kogure S (2012) Immunocytochemical studies on the effect of 405-nm low-power laser irradiation on human-derived A-172 glioblastoma cell. *Lasers Med Sci.* 27: 935–942.
- 73) Cavett W, Tucci M, Cason Z, Lemos L, England B, et al. (1997) Comparison of cellular responses induced by low level light in different cell types. *Biomed Sci Instrum* 33: 155–60.
- 74) Karu T (2003) Low Power Laser Therapy. *Biomedical Photonics Handbook* 48: CRC Press. p.48.
- 75) Gao X, Xing D (2009) Molecular mechanisms of cell proliferation induced by low power laser irradiation. *J Biomed Sci.* DOI:10.1186/1423-0127-16-4.
- 76) McBride HM, Neuspiel M, Wasiak S (2006) Mitochondria: more than just a powerhouse. *Curr Biol.* 16: 551–560.

Chapter 3

532 nm LLI recovers γ -secretase inhibitor-mediated cell growth suppression and promotes cell proliferation via Akt signaling

Contents

3.1 Introduction

3.2 Materials and Methods

3.2.1 Immunofluorescent staining method

3.2.2 Pretreatment cells with γ -secretase inhibitor (GSI)

3.2.3 Laser irradiation method

3.2.4 Cell culture of glioblastoma (A-172)

3.2.5 Statistical analysis

3.3 Results

3.3.1 Expressions of p-Akt and p-PTEN by 532 nm LLI

3.3.2 Effects of a combined application of GSI and LLI on cell proliferation

3.3.3 Effects of LLI on Intracellular Signaling Molecules under GSI

3.4 Discussion

3.5 References

3.1 Introduction

We found 532 nm LLI increased cell proliferation of A-172 cells. Then we investigated how 532 nm LLI affect to intracellular mechanisms. We focused on Notch-Pten-Akt pathway mediated by GS.

3.2 Materials and methods

3.2.1 Immunofluorescent staining method

The cells were rinsed three times with PBS after LLI. They were fixed with 4% PFA, treated with 0.1% Triton X-100 and blocked by 1% BSA-PBS. Primary antibody against phospho-Thr308-Akt (1:800, Cell Signaling), phospho-Ser473-Akt (1:800, Promega), phospho-Ser380/Thr382/383-PTEN (1:100, Cell Signaling), or A β -Amyloid (1:50, Cell Signaling) was added and left overnight at 4°C. Next day, secondary antibody (Rhodamine, FITC) was added and incubate for 3 h under room temperature. After washing with PBS, glycerol was added and cover glass was put on. Stained cells were observed by a fluorescent microscope (BZ-9000, KEYENCE, Tokyo, Japan). The center of each well was photographed with same exposure time using a 20x objective lens after focusing on cells under phase contrast. The maximum intensity in irradiated area was measured using an optional software (BZ-analysis application, KEYENCE) without applying any image enhancement. However, the haze reduction was used to make fluorescent images clearer.

3.2.2 Pretreatment cells with γ -secretase inhibitor (GSI)

DAPT, a typical agent of GSIs, was cryopreserved at 1 mM in DMSO. DAPT was added directly to FBS-DMEM medium at 25 μ M and applied to cells 3 h before LLI. DMSO (1% in the medium) showed harmless effects in preliminary experiments (data not shown).

3.2.3 Laser irradiation method

A diode laser apparatus (Nd:YVO₄, CW, 532 nm, 0–180 mW) was used. The experiment was conducted in a clean bench under 37°C and 5% CO₂. The laser beam was reflected on a mirror and introduced to cells from the top to the bottom. The averaged power was 60 mW and the irradiated area was 7.1 mm², thus the power density was 845 mW/cm². In experimental group, the center of dish or well was irradiated for 20, 40 and 60 min with an energy density of 10.1, 20.3, 30.4 \times 10² J/cm², respectively.

3.2.4 Cell culture of glioblastoma (A-172)

The human-derived glioblastoma A-172 cell line was obtained from JCRB (#0228). The cells were cultured in 25 cm² flasks with DMEM containing 10% fetal bovine serum and incubated in an atmosphere of 5% CO₂, 95% air at 37°C. The medium was changed once every three days to maintain cell growth. Trypsinization was performed using 0.1% trypsin-PBS once the cells reached confluency (10⁶ cells). Cells were plated in 35 mm dish, 96-well plates (MS-8096F, Sumitomo Bakelite Co. Ltd., Tokyo, Japan), or LAB-TEK Chamber Slide (Nalge Nunc International, New York, USA) with 10% FBS-DMEM medium at 6 \times 10³ cells/ml.

3.2.5 Statistical analysis

All values were presented as mean \pm SD. Student's two-tailed non-paired t-test and one-way ANOVA were used to analyze statistical differences between 2 groups or among multiple groups, respectively.

3.3 Result

3.3.1 Expressions of p-Akt and p-PTEN by 532 nm LLI

To examine possible involvement of Akt signaling in the LLI-mediated proliferation, we investigated Akt as well as PTEN activation (Fig. 14). Anti-phosphorylated Akt (p-Akt) antibodies detect activated (phosphorylated) Akt molecules, while anti-phosphorylated PTEN (p-PTEN) antibodies detect PTENs that removed the phosphate group from activated phosphoinositides and retained it. With 20 min LLI, the intensity of p-PTEN immunofluorescence did not change significantly ($95\pm 2\%$ of control). However, with 40 and 60 min LLI, the p-PTEN immunofluorescence intensity decreased significantly over control ($88\pm 5\%$, $p < 0.05$, for 40 min; $87\pm 3\%$, $p < 0.05$, for 60 min) ($n = 120$:4 experiments and 30 selected cells each). In contrast, p-Akt immunofluorescence intensity significantly increased ($122\pm 4\%$, $129\pm 1\%$, and $185\pm 8\%$ for 20, 40, and 60 min LLI over control, $p < 0.05$ or $p < 0.01$).

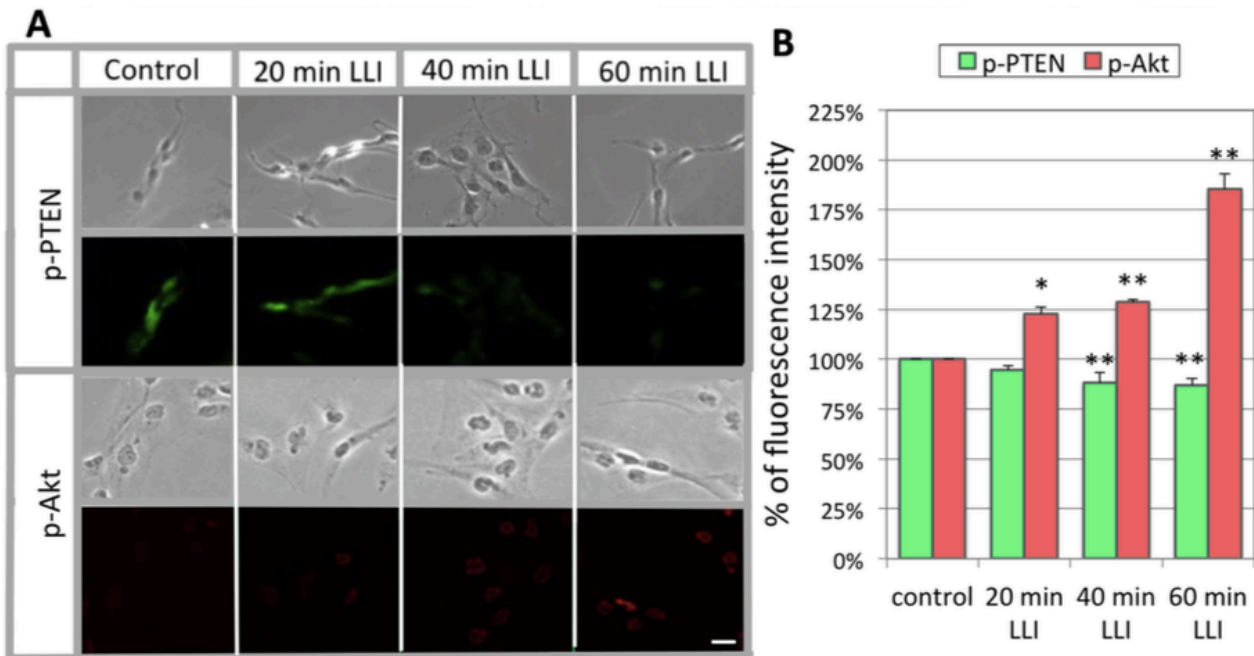


Fig. 14 Immunofluorescent staining of Akt and PTEN. A: The LLI effects on immunofluorescence staining of p-PTEN and p-Akt in cultures cells (bottom). Corresponding phase contrast micrographs are shown on top of each fluorescent image. It should be noted that tumor cells normally proliferate in high proportions and p-Akt is often highly expressed in cancer cells of different natures, whereas our result of control group shows low level of p-Akt expression due to haze reduction. Cal.: 100 μ m. B: Average fluorescence intensity for p-PTEN or p-Akt normalized to the control value. Asterisks: one-way ANOVA, * $p < 0.05$, ** $p < 0.01$.

3.3.2 Effects of a combined application of GSI and LLI on cell proliferation

DAPT, a typical agent of GSIs, has been previously shown to retard cell proliferation by reducing generation of ICN. We also tested this agent in A-172 cells in 13 experiments. At 24 h after LLI, the standardized proliferation ratios were $178 \pm 16\%$ for control group, $196 \pm 26\%$ for experimental group which received 60 min LLI only, $144 \pm 9\%$ for pretreated group with GSI, and $186 \pm 8\%$ for group received both applications, respectively. At 48 h after LLI, they were 282 ± 27 , 302 ± 37 , 168 ± 4 , and $216 \pm 16\%$, respectively (Fig. 15). There were statistical significances between some pairs of groups as shown in Fig. 15 ($p < 0.01$ or $p < 0.05$). It is worthy of note that the LLI was able to rescue the DAPT-induced reduction of cells by approximately $(186 - 144 =) 42\%$ at 24 h and $(216 - 168 =) 48\%$ at 48 h after LLI.

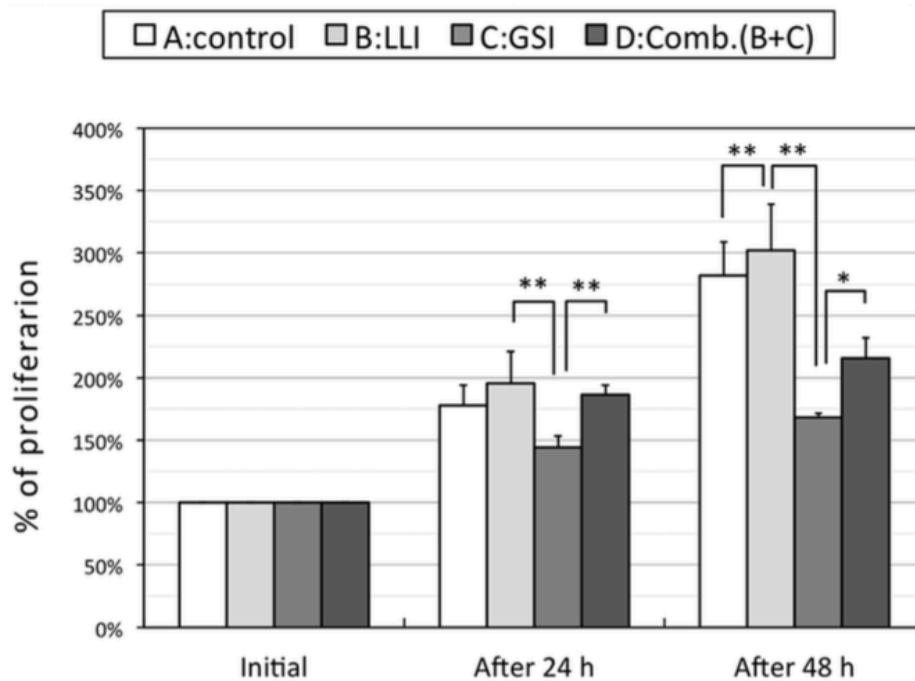


Fig. 15 Effects of LLI, DAPT and combined application of both on cell proliferation. Proliferation ratios for each group at 24 h and 48 h after LLI for control (white bars), 60 min LLI (light grey bars), DAPT (grey bars) or the combination of LLI and DAPT (dark grey bars) are shown. Asterisks: one-way ANOVA, * $p < 0.05$, ** $p < 0.01$.

3.3.3 Effects of LLI on Intracellular Signaling Molecules under GSI

Fig. 16A describes the action of GS in relation to Notch and APP processing. GS cleaves Notch as well as APP at plasma membrane, making ICN and A β , respectively. When GS is inhibited by GSI, ICN level will be reduced and PTEN expression will increase, resulting in suppression of Akt signaling pathway and in inhibition of cell proliferation and survival (Fig. 16B). Similarly, A β level will decrease as more uncleaved APP will remain.

We next tested if the LLI-mediated rescue of GSI-induced reduction in cell number (Fig. 15) involves activation of Akt and the reduction of PTEN. As described above, A-172 cells were treated with DAPT for 3 hours, exposed to LLI for 20, 40, and 60 min, and fixed at 15 min for the immunofluorescent staining of p-Akt and p-PTEN (Fig. 16C). Immunofluorescence intensity was quantified for each protein and normalized to non-DAPT treated control (Fig. 16D) (n = 120: 4 experiments and 30 selected cells each). As expected, DAPT treatment increased the expression of p-PTEN (114 \pm 3% when standardizing untreated control as 100%, p<0.01), suggesting that PTEN expression has increased due to inhibition of GS and reduction of ICN. We also examined if soluble A β is reduced by immunofluorescent staining using anti-A β antibodies. As would be expected for the inhibition of GS, A β was reduced in DAPT-treated cells (82 \pm 1%, p<0.01). We then tested if LLI could alter the expression of p-PTEN as well as A β . Simultaneous application of 20 min LLI reduced p-PTEN to the control level, but did not affect already reduced A β level. Effects of 40 and 60 min LLI were similar to 20 min LLI. These data suggest that LLI, within 20 min, acts specifically on the Notch pathway to reduce PTEN expression, but does little to the APP processing and homeostasis of A β .

Immunofluorescence intensity of p-Akt was reduced slightly from the control level in DAPT-treated cells (94 \pm 1%, p<0.01). This decrease was rescued by LLI. With 20 min LLI, the immunofluorescent staining of p-Akt was recovered to the control level. With 40 and 60 min LLI, the intensity significantly increased 112 \pm 21% (p<0.01) and 137 \pm 36% (p<0.01) above the control level, respectively. These data suggest that LLI could recover DAPT-induced reduction of p-Akt in a dose-dependent manner.

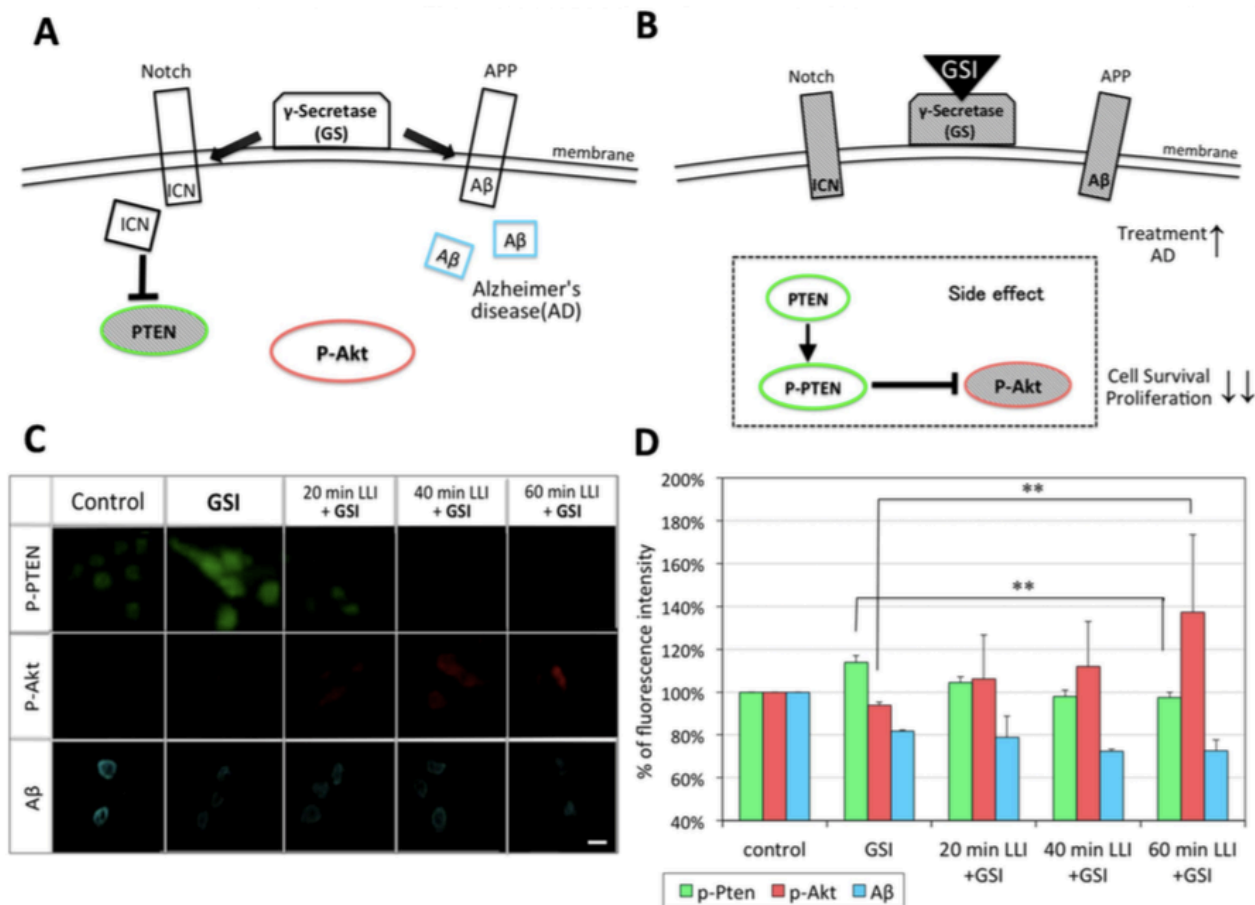


Fig. 16 Effects of LLI on the fluorescence intensities of p-Akt, p-PTEN and A β . A, B: Schematic diagrams of Notch and APP signaling pathways. GS can cleave APP and Notch, making A β and ICN, respectively (A). GSI inhibits A β expression but also inhibits ICN expression (B), a side-effect against cell survival through PTEN activation (dashed box in B). C: LLI effects on immunofluorescence staining of p-Akt, p-PTEN and A β in cells pretreated with GSI. Cal.: 100 μ m. D: Average fluorescence intensity for p-PTEN (green bars), p-Akt (pink bars) and A β (blue bars) was normalized to control. Asterisks: one-way ANOVA, ** p,0.01.

3.4. Discussion

The present study focused on the effect of LLI on the Notch-PTEN-Akt pathway in glioblastoma. We showed a reciprocal expression of p-PTEN inactivation and p-Akt activation in Fig. 14. Previous work of others showed the effects of LLI on the mitogen-activated protein kinase (MAPK) pathway⁷⁷ and the ROS-Src pathway⁷⁸. To our knowledge, this is the first to report that LLI at any wavelength influenced the Notch pathway. Previously, it was suggested that Akt plays a key role for cell survival and proliferation⁷⁹. Using FRET, it was demonstrated that 632 nm LLI increased cell proliferation via the activation of Akt signaling pathway⁸⁰. It was also reported that 632.8 nm LLI inhibits the expression of p21⁸¹, a molecule that arrests the cell-cycle, and enhances the cell-cycle progress via its phosphorylation by Akt⁸². Recent investigations implicate an important role of Akt in mitochondria for the regulation of cell growth. The expression level of Akt in mitochondria is dynamically regulated by cellular signaling activities⁸³, and Akt mediates mitochondrial protection in cardiomyocytes⁸⁴. Importantly, Akt suppresses apoptosis signaling independent of cytosolic Akt in cardiac muscle cells⁸⁵. Considering a number of studies addressing the effects of LLI on mitochondria⁸⁶, our study may have revealed Akt as an interesting link between LLI and mitochondria.

GSI has been proposed for the treatment of Alzheimer's disease because its inhibition of GS will decrease the generation of intracellular A β , a potential culprit in Alzheimer's disease⁸⁷. However, GSI treatment will also cause a side effect in healthy cells in Alzheimer's disease patients since GSI will prevent the normal processing of Notch, whose cleavage by GS at plasma membrane generates ICN, a PTEN suppressor and an Akt enhancer, promoting cell survival^{88,89}. In this study, we observed that GSI down-regulated A β and upregulated PTEN, suppressing Akt activation and depressing cell proliferation and cell survival as predicted from previous studies. We also showed that 532 nm LLI was able to decrease PTEN expression of GSI-pretreated cells and to increase Akt expression of those cells while keeping A β suppressed. We further demonstrated that the LLI rescued the depression of cell proliferation and even induced further growth. Thus, LLI may be useful to prevent the side effect in the Alzheimer's disease treatment using GSI. Future studies will examine the combined administration of GSI and 532 nm LLI in animal models of Alzheimer's disease in vivo.

3.5 References

- 77) Shefer G, Oron U, Irintchev A, Wernig A, Halevy O (2001) Skeletal muscle cell activation by low-energy laser irradiation: a role for the MAPK/ERK pathway. *J Cell Physiol* 187: 73–80.
- 78) Zhang J, Xing D, Gao X (2008) Low-Power Laser Irradiation Activates Src Tyrosine Kinase Through Reactive Oxygen Species-Mediated Signaling Pathway. *J Cell Physiol* 217: 518–528.
- 79) Kim D, Chung J (2002) Akt: Versatile Mediator of Cell Survival and Beyond. *Journal of Biochemistry and Molecular Biology* 35: 106–115.
- 80) Zhang L, Xing D, Gao X, Wu S (2009) Low-power laser irradiation promotes cell proliferation by activating PI3K/Akt pathway. *J Cell Physiol* 219: 553–562.
- 81) Shefer G, Partridge TA, Heslop L, Gross JG, Oron U, et al. (2002) Low-energy laser irradiation promotes the survival and cell cycle entry of skeletal muscle satellite cells. *J Cell Sci* 115: 1461–1469.
- 82) Azevedo LH, de Paula Eduardo F, Moreira MS, de Paula Eduardo C, Marques MM (2006) Influence of different power densities of LILT on cultured human fibroblast growth. *Lasers Med Sci* DOI 10.1007/s10103-006-0379-9.
- 83) Bijur GN, Jope RS (2003) Rapid accumulation of Akt in mitochondria following phosphatidylinositol 3-kinase activation. *J Neurochem* 87: 1427–1435.
- 84) Miyamoto S, Murphy AN, Brown JH (2008) Akt mediates mitochondrial protection in cardiomyocytes through phosphorylation of mitochondrial hexokinase-II. *Cell Death Differ* 15: 521–529.
- 85) Su CC, Yang JY (2012) Mitochondrial Aktregulated mitochondrial apoptosis signaling in cardiac muscle cells. *Am J Physiol Heart Circ Physiol* 302: 716–23.
- 86) Karu T (2008) Mitochondrial Signaling in Mammalian Cells Activated by Red and Near-IR Radiation. *Photochem Photobiol* 84: 1091–1099.
- 87) Takasugi N, Tomita T, Hayashi I, Tsuruoka M, Niimura M, et al. (2003) The role of presenilin cofactors in the gamma-secretase complex. *Nature* 422: 438–441.

- 88) Panza F, Solfrizzi V, Frisardi V, Capurso C, D'Introno A, et al. (2009) Disease modifying approach to the treatment of Alzheimer's disease: from alpha-secretase activators to gamma-secretase inhibitors and modulators. *Drugs Aging* DOI: 10.2165/11315770-000000000-00000.
- 89) Chan SM, Weng AP, Tibshirani R, Aster JC, Utz PJ (2007) Notch signals positively regulate activity of the mTOR pathway in T-cell acute lymphoblastic leukemia. *Blood* 110: 278–286.

Chapter 4

532 nm LLI facilitates migration on NSPCs derived from E14 GE whereas promotes proliferation on NSPCs derived E10 FB

Contents

4.1 Introduction

4.2 Materials and Methods

4.2.1 Neural Stem/Progenitor Cell (NSPC) primary culture

4.2.2 Proliferation analysis and migration analysis in culture

4.2.3 Western blotting

4.2.4 Laser irradiation method

4.2.5 Statistical Analysis

4.3 Results

4.3.1 LLI effect on cell proliferation of cultured NSPCs derived from E10 forebrain

4.3.2 LLI effect on cell migration of cultured NSPCs derived from E14 MGE

4.3.3 LLI effect on pAkt and Akt expression of cultured cell

4.4 Discussion

4.5 References

4.1 Introduction

Since 532 nm LLI increased A-172 cells in chapter 3, we investigated whether 532 nm LLI promote proliferation of cultured NSPCs. NSPCs were purified from mouse embryo.

4.2 Materials and methods

4.2.1 Neural Stem/Progenitor Cell (NSPC) primary culture

NSPC primary culture was performed according to the neurosphere methods. During the development of mouse cerebral cortex, the progenitor amplification occurs from E9 and neurogenesis starts from E11. After E18, the genesis of astrocytes and oligodendrocytes occurs along with maturation of neurons. Therefore, primary NSPCs were prepared from the MGE or cortical cerebral wall of E10.5, E14.5 and E16.5 mouse forebrain. Pregnant mice were sacrificed by cervical dislocation, embryos were removed, and their brains were dissected in PBS on ice. The brain tissue from each embryo was incubated in 2.5% trypsin for 30 min at 37°C water bath and then transferred to culture medium consisting of DMEM/F12 (Table 3) supplemented with 100 µg/ml transferrin, 30 M selenium, 10 µg/ml heparin, 25 µg/ml insulin, and 20 ng/ml basic fibroblast growth factor (Table 4). The cells were cultured at a density of 1×10^5 cells/ml in uncoated plastic 35 mm dish. The next day, suspension cells along with the medium was placed in a new dish to exclude differentiated cells adhered to the bottom of the dish, and the same volume of new medium was mixed. After NSPCs had been cultured for 3 days, resulting in forming neurospheres, each neurosphere was transferred to 96-well plates with round-bottom (Sumitomo Bakelite Co. Ltd., Tokyo, Japan), and then was used for LLI experiment. When neurospheres were transferred under the microscope by a pipette, we selected those that are non-adherent and sphere-shaped as NSPCs.

Table 3 DMEM/F12 Medium

Contents	Store	Volume
DMEM (powder)	4°C	3.3 g
F12 (powder)	4°C	3.3 g
Streptomycin	RT	0.050 g
Penicillin	RT	0.015 g
HEPES	RT	1.75 g
NaHCO ₃	RT	1.85 g
ddH ₂ O	RT	450 ml

*After adjust pH7.0, add H₂O till 500 ml

Table 4 Supplement

Contents	Concentration		Volume
	Stock	Final	
Transferrin	30 mg/ml	100 μg/ml	13.32 μl
Selenium	3 μM	30 nM	40 μl
Heparin	2 mg/ml	10 μg/ml	20 μl
Insulin	25 mg/ml	25 μg/ml	4 μl
bFGF	20 μg/ml	20 ng/ml	4 μl
DMEM/F12			4 ml

*Add just before using medium

4.2.2 Proliferation analysis and migration analysis in culture

Cell proliferation rate was measured by Cell Counting Kit-8 (CCK-8) colorimetric assay (Dojindo Co. Tokyo, Japan). At 24 or 48 hours after LLI, 10 μl of the CCK-8 solution was added to each well. The cells were incubated at 37°C for 4 hours. The absorbance at 450 nm was measured using a microplate reader (model 680, BIO RAD, Tokyo, Japan). Neurospheres were photographed with a microscope (BZ-9000, KEYENCE, Tokyo, Japan), and then single cells obtained from trituration of neurospheres were stained with DAPI and photographed.

For migration assay, polycarbonate membrane inserts with 8 μm pore size (Corning Trans-well: Sigma) was used. After LLI, cells on the lower side of the insert filter were fixed with 4% paraformaldehyde for 40 min, permeabilized with 0.1% Triton X-100 for 5 min, and preincubated with blocking solution (1% bovine serum albumin, 1% goat serum in PBS) followed by a primary antibody against GAD67 (1:1000, Millipore) incubation overnight at 4°C and a secondary antibody (Rhodamine- or FITC-conjugated) incubation for 3 hours under room temperature. Cells were stained with Hoechst 33342 (Sigma) for 20 min. The number of cells on the lower side of the filter was counted under a microscope. Images were analyzed using an optional software for neurosphere size and the number of nuclei.

4.2.3 Western blotting

Samples from cultured cells were homogenized with a lysis buffer (10 mM Tris HCl, 1 mM EDTA, 1 mM sodium orthovanadate, 1mM PMSF, 2.5 mM sodium pyrophosphate, 1 mM β -glycerophosphate, protease inhibitor cocktail (Sigma), and 1% Triton X-100). Protein concentration was determined by BCA assay or micro BCA assay (Thermo). Homogenates were mixed with a 5x sample buffer: 312.5 mM Tris (pH6.8), 50% glycerol, 10% SDS, 5% β -mercaptoethanol, 0.00625% bromophenol blue. An equivalent amount of samples were loaded and separated by 10% polyacrylamide gel electrophoresis and transferred to PVDF transfer membranes (Immoblin-P, Millipore). Membranes were blocked with a blocking solution containing 5% non-fat dry milk (SACO Foods) and 5% protease-free bovine serum albumin (EQUATECH-BIO) in TBS-T (50 mM Tris-buffered saline with 0.1% (v/v) Tween-20)) for 60 min at room temperature. After washing with TBS-T, membranes were incubated with primary antibodies (mouse anti-phospho-Akt, 1:1000, CST; mouse anti-Akt, 1:1000, CST; mouse anti- β -Actin, 1:1000, rabbit anti-GAPDH, 1:1000, Sigma) diluted in same the blocking solution at 4°C overnight. Following washing with TBS-T, membranes were incubated with secondary antibodies (HRP-conjugated anti-rabbit IgG, Jackson; HRP-conjugated anti-mouse IgG, Jackson) at 1:1000 for cultured cells. The immunoblots were detected by chemiluminescence (ECL Prime Western blotting detection reagent, BioRad) with a FAS1000 imaging system (Fujifilm, Tokyo, Japan). The optical density of protein bands was quantified using gel analysis function of NIH Image J software.

4.2.4 Laser irradiation method

The experiment of laser irradiation was conducted in a clean bench. Two hot plates were put in clean bench to heat until 37°C and the hot plates switched on keeping warm to incubate. The CulturePal CO₂ (Cosmobio Co. Tokyo, Japan) and the Gas-tight container were used in order to keep 5% CO₂ during LLI irradiation. Then pre-experiment was carried out whether cells are able to culture under this environment or not. The cultured cells put in CulturePal CO₂ which is instrument as a transport for cultured cells. The condition of CulturePal CO₂ under the 37°C at clean bench was compared with CO₂ incubator (normal condition). The cell morphology and proliferation in the CulturePal CO₂ were same as normal condition in CO₂ incubator. A diode laser apparatus (Nd:YVO₄, CW, 532 nm, 0–180 mW) was placed in the clean bench. The laser beam was reflected on a mirror and introduced to cells from the top of the dish. The averaged power was 60 mW measured by power meter, and the irradiated area was 7.1 mm², the calculated power density was 845 mW/cm². In experimental group, the center of dish or well was irradiated for 20, 40 and 60 min with an energy density of 10.1, 20.3, 30.4×10² J/cm², respectively.

4.2.5 Statistical Analysis

Values were presented as mean ± SD or mean ± SEM as indicated. Student's two-tailed unpaired t-test or non-parametric Kolmogorov-Smirnov 2-sample test (KS test) was used to analyze statistical differences between 2 groups or among multiple groups, respectively.

4.3 Result

4.3.1 LLI effect on cell proliferation of cultured NSPCs derived from E10 forebrain

To examine the LLI effects on NSPCs of different types, we prepared neurospheres from E10 forebrain, which generate excitatory neurons, and those from E14 MGE, which generate inhibitory GABAergic neurons (Fig. 17A). Using the CCK-8 assay, which allows biochemical determination of cell proliferation rates, we observed that 60 min LLI promoted proliferation of neurospheres derived from E10 forebrain but not derived from E14 MGE (Fig. 17B). Additionally, LLI significantly increased the number of dissociated cells prepared from E10 forebrain compared with control as determined by DAPI staining (Fig 17C). These data suggest that LLI induces proliferation of NPSCs that generate excitatory neurons, but not NPSCs that become GABAergic neurons, supporting the idea that LLI induces migration, not proliferation, of GABAergic cells in A1.

4.3.2 LLI effect on cell migration of cultured NSPCs derived from E14 MGE

We then examined whether LLI can induce cell migration in vitro. NSPCs were collected from E16 cortex (Fig 18A), which included excitatory and inhibitory NSPCs. Neurospheres were cultured in trans-well plates and received LLI from above (Fig 18B). At 48 h after LLI, GAD67-positive cells, but not GAD67-negative cells, were found beneath the trans-well membrane only in LLI group (Fig 18C). LLI increased the number of GAD67-positive cells about 3-fold. No GAD67-negative cell was found to be migrating, however. These data suggest that LLI could induce cell migration on inhibitory GABAergic neurons, which is consistent with in vivo experiments above.

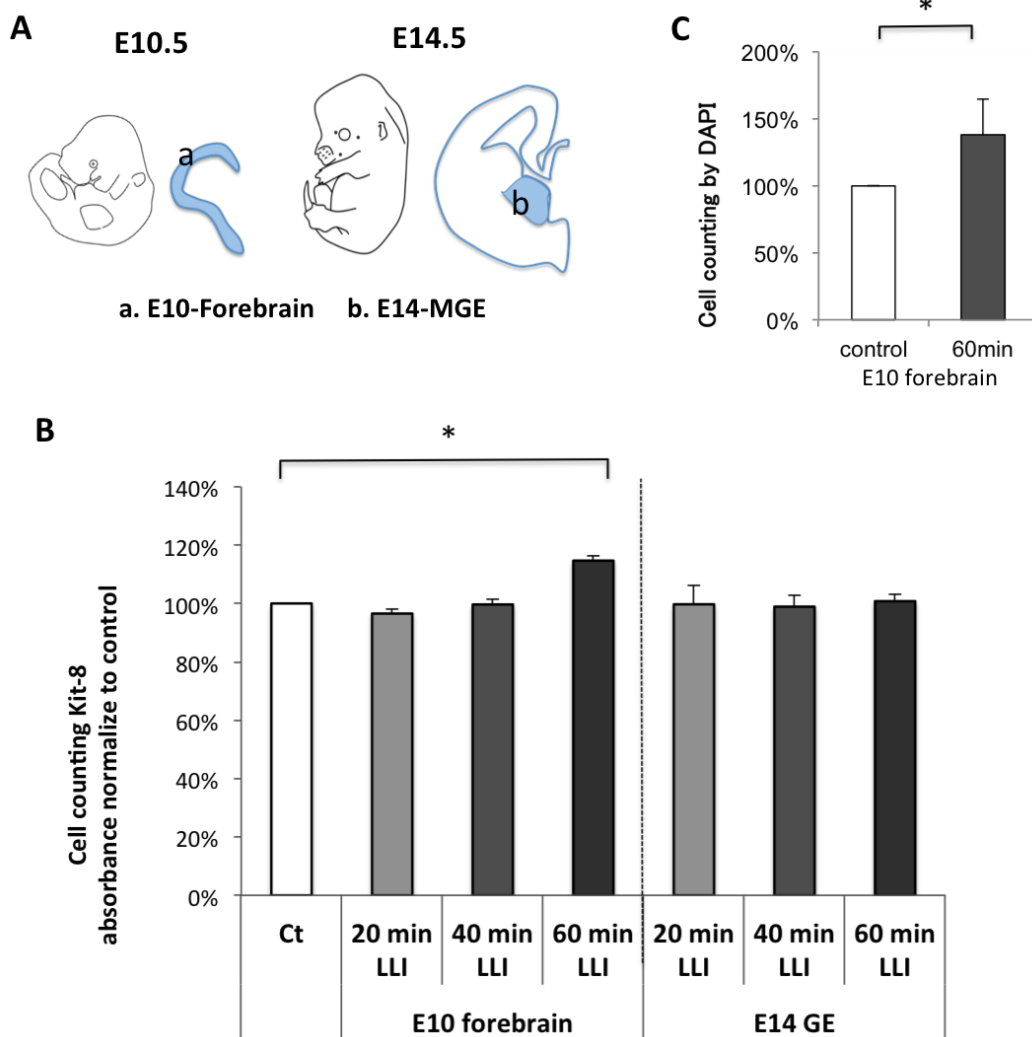


Fig. 17 LLI effects on proliferation of NSPC cells from E10 forebrain and E14 MGE. A: Location of brain parts dissected for making neurosphere of NSPCs. “a” shows cortical wall of E10 forebrain, which generates excitatory neurons, whereas “b” shows E14 MGE, which generates GABAergic neurons. B: CCK-8 assay to show biochemically cell proliferation for different duration of LLI (mean \pm SD, $n = 4$ for each duration, t-test, $*p < 0.05$). The non-irradiated group was standardized as 100%. C: Cell counting of DAPI staining to clarify the increase in cell number following the dissociation from neurospheres. LLI significantly promoted proliferation (mean \pm SD, $n = 5$, t-test, $*p < 0.05$).

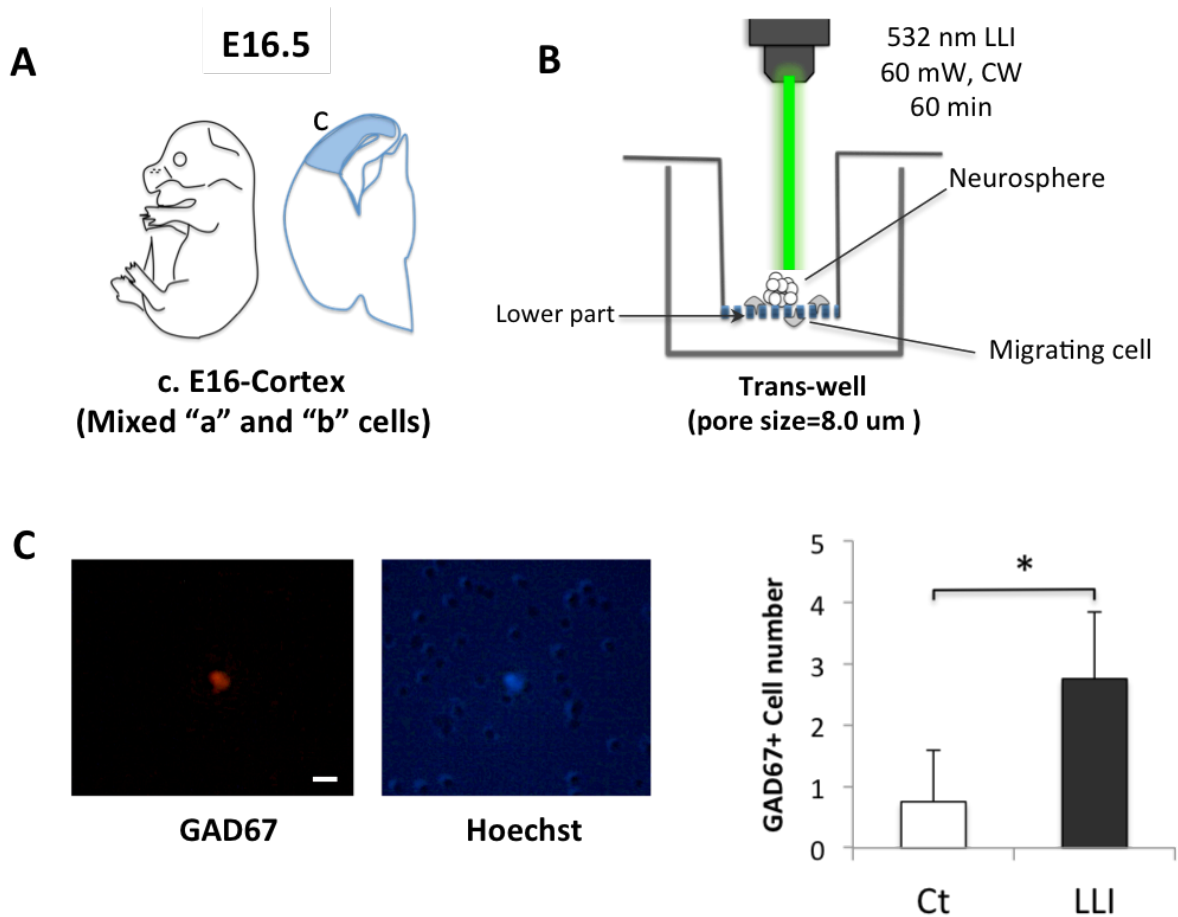


Fig. 18 Trans-well migration experiments. A: Location of brain parts dissected for making neurospheres of NSPCs. Label "c" shows the cortex of E16, which includes NSPCs of excitatory and GABAergic neurons. B: Method of trans-well migration test. Bottom membrane of inserted trans-well has pores of 8 µm diameter. Neurospheres derived from "c" were placed on insert trans-well, and 532 nm laser was irradiated from above the media. Cells were fixed by 4% PFA at 48 h after LLI. C: A cell that moved through the pores stained by GAD67 (red) and Hoechst (blue). Holes in the Hoechst image are the pores of trans-well. Scale bar: 10 µm. Double positive cells were found only in the LLI experimental group (mean ± SD, n = 4, t-test *p < 0.05).

4.3.3 LLI effect on pAkt and Akt expression of cultured cells

To test whether Akt is activated in GABAergic NSPCs, the level of phosphorylated Akt (pAkt) and Akt expressions on cultured NSPCs were examined using Western blot techniques (Fig 19B). LLI increased Akt expression but induced little changes in the phosphorylation state of Akt on NSPCs derived from the E10 forebrain (Fig 19C).

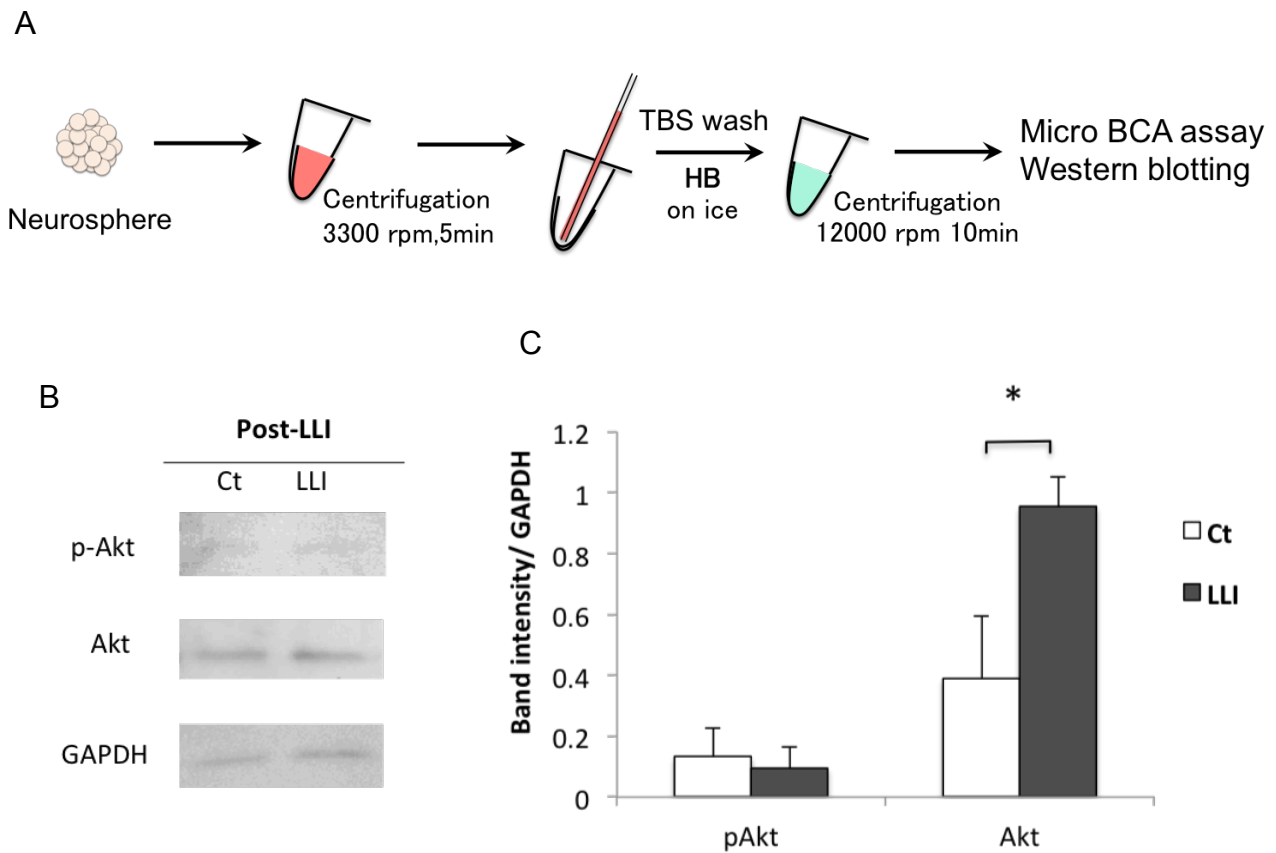


Fig. 19 LLI effects on pAkt and Akt expression of cultured cells. A: schematic diagram of making sample in vitro. B: Western blot analysis of neurosphere lysates from post-LLI (4 hours) of E10 forebrain. C: Quantification of blots. Each blot intensity was normalized to GAPDH of loading control (mean \pm SD, n = 3, t-test *p < 0.05).

4.4 Discussion

We observed that 60 min 532 nm LLI promoted proliferation of neurospheres derived from E10 forebrain but not derived from E14 MGE. LLI induces proliferation of NPSCs that generate excitatory neurons, but not NPSCs that become GABAergic neurons. We then examined whether LLI can induce cell migration in vitro. At 48 h after LLI, GAD67-positive cells, but not GAD67-negative cells, were found beneath the trans-well membrane only in LLI group. LLI increased the number of GAD67-positive cells. In addition, Akt and pAkt in neurosphere were enhanced by 532 nm LLI.

How could the 532 nm LLI affect Akt signaling pathway? The mechanism of LLI including other wavelength may depend on photoacceptors in the mitochondrial respiratory chain^{90, 91}). However, considering that LLI induced different biological effects of cell proliferation on different cell types such as glioblastoma, skin cells⁹²), and NSPCs in this study, it is difficult to conclude that the regulation by mitochondrial photoacceptors is the only mechanism underlying LLI-mediated cell proliferation, differentiation and migration.

Another possibility cannot be excluded, such as direct photochemical influence on the extracellular factors that can provide molecular cues to those developmental events. There are many reports that extrinsic cues, including cell-cell interactions and secreted molecules, are key determinants of NSPC fate. Neurotrophic factors such as platelet-derived growth factor, brain-derived neurotrophic factor, and glial cell line-derived neurotrophic factor are known to promote neuronal fate, where the selective expansion of neuronal progenitors and the enhancement of the survival of neurons (or their progenitors) have been reported⁹³⁻⁹⁶). Several reports also showed that LLIs affect the release of various types of growth factors to induce beneficial effects⁹⁷⁻⁹⁹). Therefore, it is possible that 532 nm LLI influences the Akt signaling pathway via activation or inactivation of growth factors or cytokines.

4.5 References

- 90) Karu T (2003) *Low Power Laser Therapy*. Biomedical Photonics Handbook 48: CRC Press.
- 91) Gao X, Xing D (2009) Molecular mechanisms of cell proliferation induced by low power laser irradiation. *J Biomed Sci*. doi: 10.1186/1423-0127-16-4
- 92) Moore P, Ridgway TD, Higbee RG, Howard EW, Lucroy MD (2005) Effect of Wavelength on Low-Intensity Laser Irradiation-Stimulated Cell Proliferation In Vitro. *Lasers Surg Med*. 36(1):8–12. PMID: 15662631
- 93) Hirabayashi Y, Itoh Y, Tabata H, Nakajima K, Akiyama T, et al. (2004) The Wnt/beta-catenin pathway directs neuronal differentiation of cortical neural precursor cell. *Development* 131:2791–2801. PMID: 15142975
- 94) Arsenijevic Y, Weiss S (1998) Insulin-like growth factor-I is a differentiation factor for postmitotic CNS stem cell-derived neuronal precursors: Distinct actions from those of brain-derived neurotrophic factor. *J Neurosci* 18:2118–2128. PMID: 9482798
- 95) Pozas E, Ibanez CF (2005) GDNF and GFRalpha 1 promote differentiation and tangential migration of cortical GABAergic neurons. *Neuron* 45:701–713. PMID: 15748846
- 96) Guillemot F (2007) Cell fate specification in the mammalian telencephalon. *Prog Neurobiol* 83:37–52. PMID: 17517461
- 97) Reddy GK, Stehno-Bittel L, Enwemeka CS (2001) Laser photostimulation accelerates wound healing in diabetic rats. *Wound Repair Regen* 9:248–255. PMID: 11472621
- 98) Webb C, Dyson M, Lewis W (1998) Stimulatory effect of 660 nm low level laser energy on hypertrophic scar-derived fibroblasts: possible mechanisms for increase in cell counts. *Lasers Surg Med* 22: 294–301. PMID: 9671996
- 99) Vinck EM, Cagnie BJ, Cornelissen MJ, Declercq HA, Cambier DC (2003) Increased fibroblast proliferation induced by light emitting diode and low power laser irradiation. *Lasers Med Sci* 18:95–99. PMID: 12928819

Chapter 5

532 nm LLI facilitates migration of GAD67 positive NSPCs in adult neocortex

Contents

5.1 Introduction

5.2 Materials and Methods

5.2.1 Transient mild ischemia

5.2.2 Laser Irradiation Method

5.2.3 Triphenyltetrazolium chloride (TTC) staining

5.2.4 Western blot analysis

5.2.5 Immunohistochemistry

5.2.6 Statistical Analysis

5.3 Results

5.3.1 Effects of transcranial LLI on cell migration of NSPCs induced by CCAO

5.3.2 Effects of transcranial LLI on pAkt and Akt expression in mouse cortex

5.4 Discussion

5.5 References

5.1 Introduction

We investigated whether transcranial LLI affect NSPCs in adult mouse brain. 532 nm laser was irradiated after surgery of mild ischemia due to induce proliferation of NSPCs in layer 1 of cortex.

5.2 Materials and Methods

We performed all experiments in accordance with the Declaration of Helsinki and the Guidelines of Animal Use Committee at Soka University. The name of Committee which approved this study plan is The Soka Bioethics Committee for Life-science. Animals were housed in facilities with a 12/12 h light/dark cycle. For in vivo or in vitro experiments, the adequate procedures including anesthetics and methods of sacrifice so as to make the suffering at the lowest level were approved by the Committee and described in each section.

5.2.1 Transient mild ischemia

Adult FVB mice (>60 postnatal days) were anesthetized with N₂O/O₂ gas, placed on a heating pad with supine position. A midline of the neck was opened, and common carotid artery (CCA) was separated from the surrounding tissue. Then bilateral CCAs were occluded by floss for 10 min (experimental group) or not occluded (sham control group). After suturing, 2% lidocaine was applied, and waited until awakening (Fig. 20).

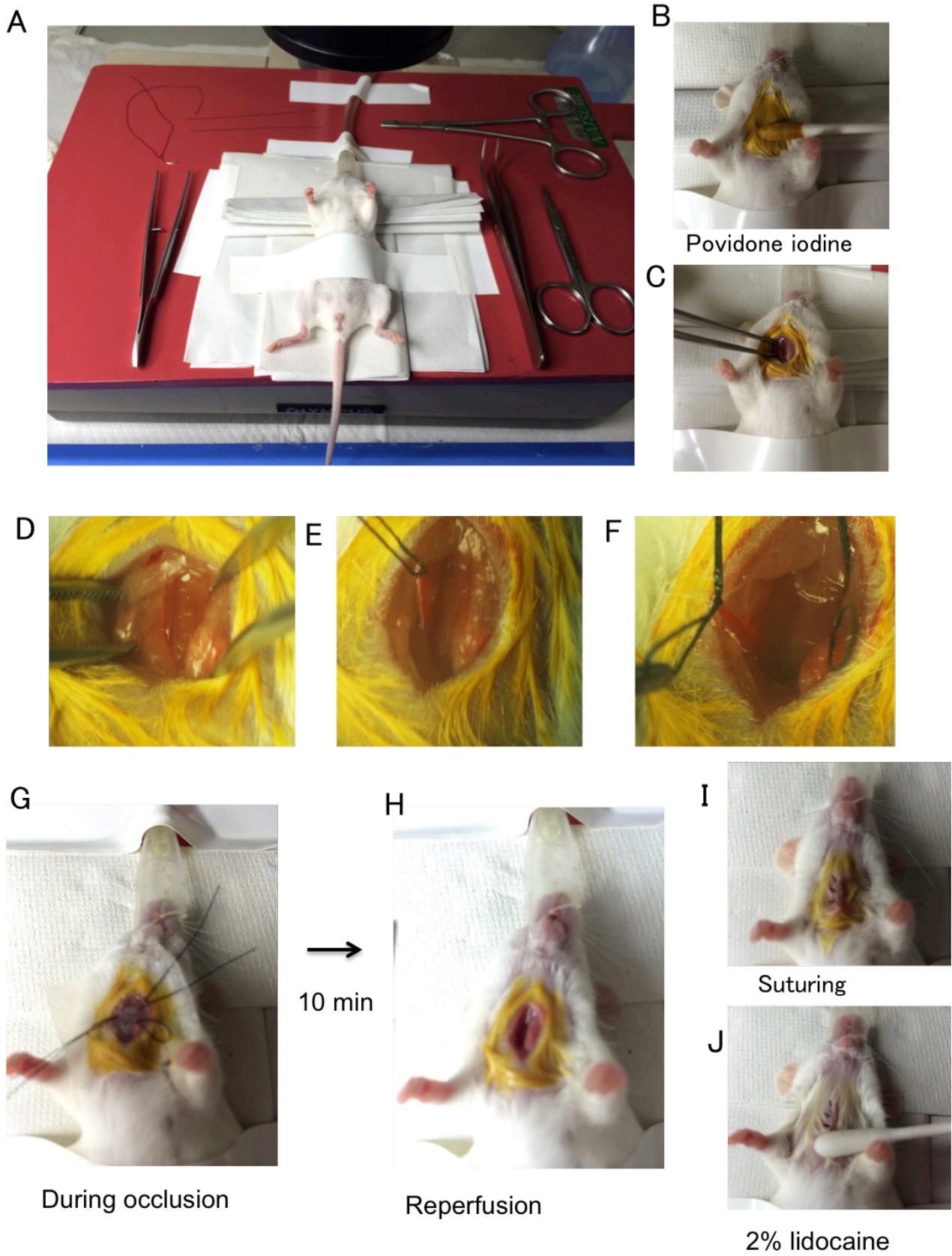


Fig. 20 Surgery of CCAO in FVB mouse. A: instrument for surgery, B–F: CCAO surgery. G, H: occlusion, I: suturing. J: swabbing the 2% lidocaine to relief of the pain.

5.2.2 Laser Irradiation Method

A diode laser apparatus (Nd:YVO₄, CW, 532 nm, 0–180 mW: SUWTECH, LDC-2500, China) was used in all experiments. The power measured in front of irradiated cortical surface was 60 mW on average and the irradiated area was 7.1 mm²; thus the power density was 845 mW/cm². Irradiation time was 60 min for experiments in vivo and 20, 40 and 60 min for experiments in vitro with an energy density of 10.1, 20.2, 30.3×10² J/cm², respectively. For in vivo experiments, FVB mice were anesthetized with a mixture of nitrous oxide and oxygen gas (2:3), and fixed on a stereotaxic apparatus. LLI was made perpendicular to the surface of the temporal skull over the left auditory cortex, while non-irradiated right auditory cortex was used as a control.

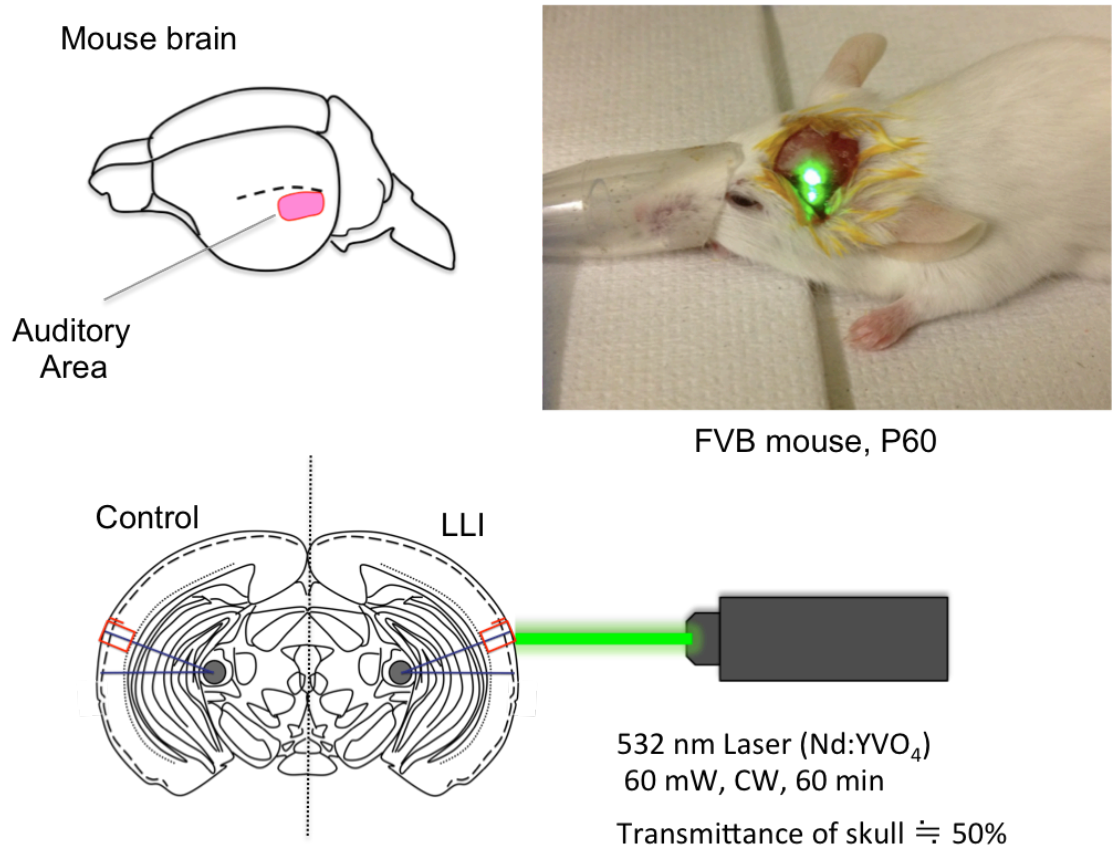


Fig. 21 LLI on FVB mouse brain

5.2.3 Triphenyltetrazolium chloride (TTC) staining

TTC (triphenyltetrazolium chloride, Wako) staining was used to detect cell death. Briefly, mice were decapitated after anesthetized with halothane. Brain was immediately taken out from the skull and placed into an iced PBS for 15 min. Brain was sliced in 2 mm thickness by a brain slicer on ice. Brain slices were incubated in 2% TTC in PBS at 37°C for 10 min. 10% formaldehyde was used in order to fix the stained brain slices.

5.2.4 Western blotting

Samples from brain block tissues of auditory area cortex or cultured cells were homogenized with a lysis buffer (10 mM Tris HCl, 1 mM EDTA, 1 mM sodium orthovanadate, 1mM PMSF, 2.5 mM sodium pyrophosphate, 1 mM β -glycerophosphate, protease inhibitor cocktail (Sigma), and 1% Triton X-100). Protein concentration was determined by BCA assay or micro BCA assay (Thermo). Homogenates were mixed with a 5x sample buffer: 312.5 mM Tris (pH6.8), 50% glycerol, 10% SDS, 5% β -mercaptoethanol, 0.00625% bromophenol blue. An equivalent amount of samples were loaded and separated by 10% polyacrylamide gel electrophoresis and transferred to PVDF transfer membranes (Immoblin-P, Millipore). Membranes were blocked with a blocking solution containing 5% non-fat dry milk (SACO Foods) and 5% protease-free bovine serum albumin (EQUATECH-BIO) in TBS-T (50 mM Tris-buffered saline with 0.1% (v/v) Tween-20) for 60 min at room temperature. After washing with TBS-T, membranes were incubated with primary antibodies (mouse anti-phospho-Akt, 1:1000, CST; mouse anti-Akt, 1:1000, CST; mouse anti- β -Actin, 1:1000, rabbit anti-GAPDH, 1:1000, Sigma) diluted in same the blocking solution at 4°C overnight. Following washing with TBS-T, membranes were incubated with secondary antibodies (HRP-conjugated anti-rabbit IgG, Jackson; HRP-conjugated anti-mouse IgG, Jackson) at 1:10000 for brain tissue. The immunoblots were detected by chemiluminescence (ECL Prime Western blotting detection reagent, BioRad) with a FAS1000 imaging system (Fujifilm, Tokyo, Japan). The optical density of protein bands was quantified using gel analysis function of NIH Image J software.

5.2.5 Immunohistochemistry

For the analysis with 5-ethynyl-2'-deoxyuridine (EdU), animals were intraperitoneally injected with EdU (50 mg/kg mouse) once after LLI. At 4 hours or 5 days after the LLI, animals were deeply anesthetized with urethane (1.2 g/kg; Sigma) and xylazine (13 mg/kg; Sigma), and sacrificed by perfusion with ice-cold PBS and 4% PFA. Brain was removed and post-fixed in 4% PFA for 2 hours at 4°C. After washing with PBS, coronal sections were prepared at 50 µm thickness containing the auditory field as identified by Paxino and Franklin's mouse atlas. Sections were heat-treated using a water bath with sodium citrate buffer (pH 6) for 30 min at 80°C for antigen retrieval. To detect EdU-incorporated cells using an imaging kit (Click-iT EdU 647, Invitrogen), brain sections were washed twice with 3% BSA in PBS, permeabilized with 0.5% Triton X-100 in PBS, washed again twice with 3% BSA in PBS, then incubated with a Click-iT reaction cocktail (Table 5). Next, for staining with mouse primary antibodies, sections were incubated for 1 hour in M.O.M. Mouse Ig blocking reagent (Vector) and then in mouse anti-GAD67 primary antibody (1:1000, Millipore) in the same blocking reagent. After washing with PBS, they were incubated with goat blocking solution (5% goat serum, 0.3% Triton X-100 in PBS) for 90 min and then rocked overnight with a rabbit polyclonal antibody against Ki67 in the blocking reagent at 4°C. The sections were washed with PBS and incubated with secondary antibodies (Alexa488-anti-rabbit or Cy3-anti-mouse) for 90 min at room temperature. Finally, nuclei were stained with 5 µg/ml Hoechst 33342 (Sigma) and mounted on microscope slides using a fluorescence anti-fade medium (Vector Laboratories). After imaging, fluorescence positive cells in all sections were counted.

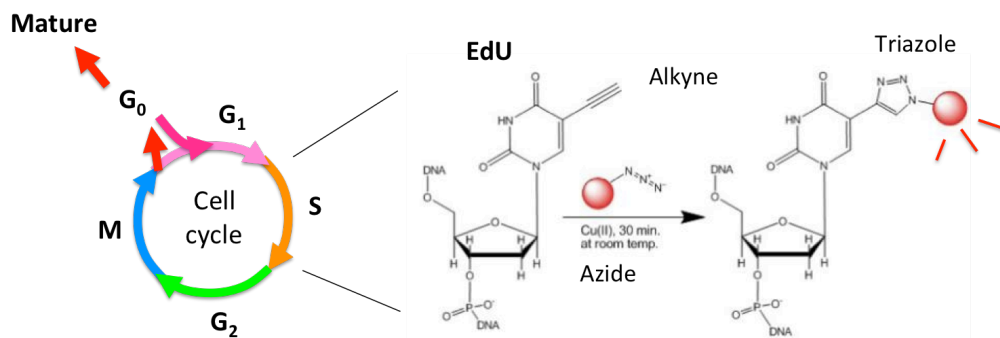


Fig. 22: Principle of Click-iT EdU staining (Invitrogen). EdU is incorporated during S-phase in cell cycle. Alkune react with Azide.

Table 5 Click-iT Reaction cocktail

Order* ³	Reaction components	1 well	5 well	24 well
1	1x Click-iT Reaction Buffer	176 μ l	880 μ l	4224 μ l
2	Copper protectant: CuSO ₄	4 μ l	20 μ l	96 μ l
3	Alexa Fluor picolyl azide	0.5 μ l	2.5 μ l	12 μ l
4	1x Reaction Buffer additive (From Step 5)	20 μ l	100 μ l	480 μ l
	Total volume	200.5 μ l	1002.5 μ l	4812 μ l

*³Note: Add the ingredients in the order listed in the table.

5.2.6 Statistical Analysis

Values were presented as mean \pm SD or mean \pm SEM as indicated. Student's two-tailed un-paired t-test or non-parametric Kolmogorov-Smirnov 2-sample test (KS test) was used to analyze statistical differences between 2 groups or among multiple groups, respectively.

5.3 Results

5.3.1 Effects of transcranial LLI on cell migration of NSPCs induced by CCAO

We first examined the influence of LLI on proliferated NSPCs induced by mild ischemia. Common carotid artery (CCA) was occluded for 10 min bilaterally, and 24 hours later, transcranial LLI was made to one side of cranial surface at the stereotaxically determined location of primary auditory cortex (A1) so as to avoid LLI on the contralateral side (i.e. control side; Fig 23A). TTC staining indicated that neither LLI for 60 min nor bilateral CCA occlusion for 10 min induced cell death compared with non-occlusion of sham control (Fig 23B). To determine if LLI induces cell proliferation, mice were injected with EdU (50 mg/kg mouse, i.p.) at the end of 60 min LLI and sacrificed by PFA perfusion 4 hours or 5 days after LLI (Fig 23C). Fluorescent labeling of EdU along with immunofluorescence co-staining against a proliferating cell marker Ki67 and an inhibitory neuron marker glutamic acid decarboxylase 67 (GAD67) showed that newly generated EdU positive cells that are also GAD67- and Ki67-immunopositive cells were present 4 hours after LLI (Post-LLI, Fig 23D). These cells are considered to be proliferating GABAergic cells generated after LLI and EdU injection. Such cells were found mostly in layer 1 of A1 [Control: 66.10 ± 33.30 cells/mm³, 4h post-LLI: 100.89 ± 30.39 cells/mm³ (t-test, $p = 0.528$)] at this time point. In addition, we could not find any EdU positive and GAD67 positive cells in non-occluded sham control (3 experiments). This result implicates that proliferation of NSPCs in the mouse cortex is promoted by mild ischemia as in the rat cortex.

We then looked for the effect of LLI on migration of proliferated cells. After 5 days of LLI, the number of EdU and GAD67 positive, but Ki67 negative, (EdU+/GAD+/Ki67-) cells was counted in each layer in irradiated side and control side of A1 (Fig 23E). The laminar distribution pattern in LLI and control group was statistically examined using the non-parametric KS 2-sample test (Fig 23F), which demonstrated significant difference between the two groups ($n = 4$, $p < 0.01$). The cumulative fractions from layer 1 to layer 4 showed a large difference (38.2%: 70.7% in control vs 32.6% in LLI) and those from layer 5 to layer 6 also showed an opposite difference (-38.1%: 29.3% in control vs 67.4% in LLI). Given that the total cell number in all layers combined showed no significant difference (Fig 23G), these data suggest that LLI induced “migration” of EdU positive cells from layer 1 to the deep layers.

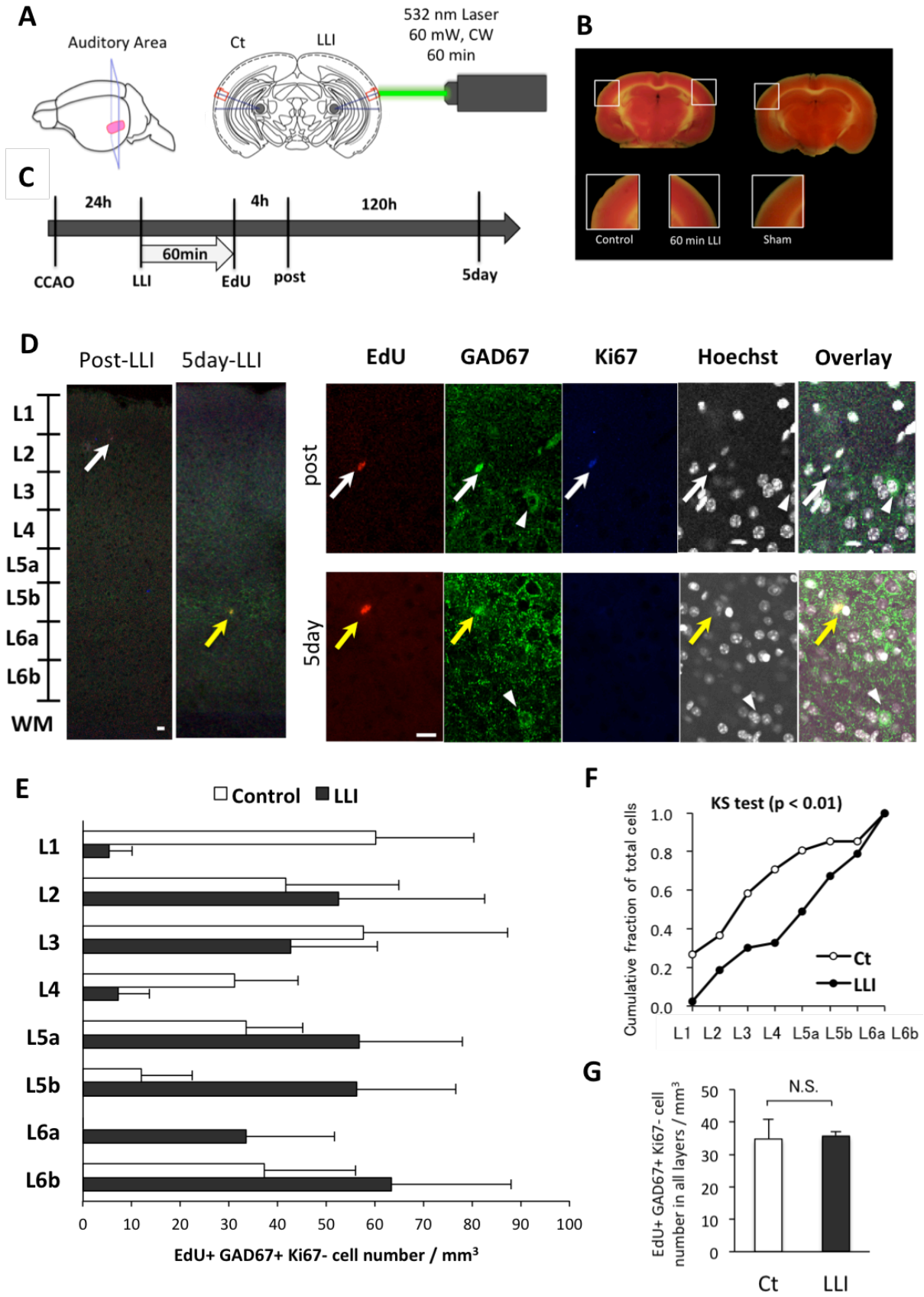


Fig. 23 Effects of transcranial LLI on cell migration of NSPCs. A: Scheme of LLI treatment to adult mouse brain. Auditory cortical area was irradiated on the left side of the cortex through cranium. The opposite hemisphere was used as a control. B: TTC staining for detecting cell death. LLI after the mild occlusion of CCA (CCAO) did not induce cell death (left) compared with sham control (right). C: Protocol for in vivo experiments from CCAO to immunostaining. Brains were fixed at 4 h and 5 days after LLI. D: Photographs of each immunostaining at post-LLI (4 hours) and 5 days after LLI. EdU, GAD67 and Ki67 positive cells (white arrow) were found in layer 1 of post-LLI sections. EdU and GAD67 positive cells but Ki67 negative cells (yellow arrow) were found in deep layer at 5 days after LLI. GAD67 positive, EdU and Ki67 negative cell (arrowhead) is a mature inhibitory neuron. Scale bars: 10 μ m. E: The laminar pattern of the cell density (mean \pm SEM, n = 4) of EdU and GAD67 positive, Ki67-negative cells from layer 1 to 6 was significantly different between LLI and control groups (KS test, $p < 0.01$). F: Cumulative fraction of total cells for non-parametric KS 2-sample test. Each accumulative curve shows higher distribution in layer 1–4 in control group, while does in layer 5–6 in LLI group. G: Total cell density of EdU and GAD67 positive and Ki67 negative (EdU +/GAD67+/Ki67-) cells did not differ between control and LLI groups.

5.3.2 Effects of transcranial LLI on pAkt and Akt expression in mouse cortex

To find possible molecular mechanisms of LLI-induced migration of GAD67-positive NSPCs, we examined the expression of phosphorylated Akt (pAkt) and Akt. Auditory cortex treated with LLI was homogenized at 4 hours and 2 days after LLI (Fig. 24). Western blot analysis was performed for pAkt, Akt and GAPDH (Fig 24B), and their blots were quantified. When normalized to GAPDH (loading control), both pAkt and Akt expressions showed significant increase when 4 hours post-LLI was compared with non-irradiated control (Fig 24C), but not significant difference was seen at 2 days after LLI. These data may indicate that pAkt and Akt are upregulated soon after LLI to initiate migration process.

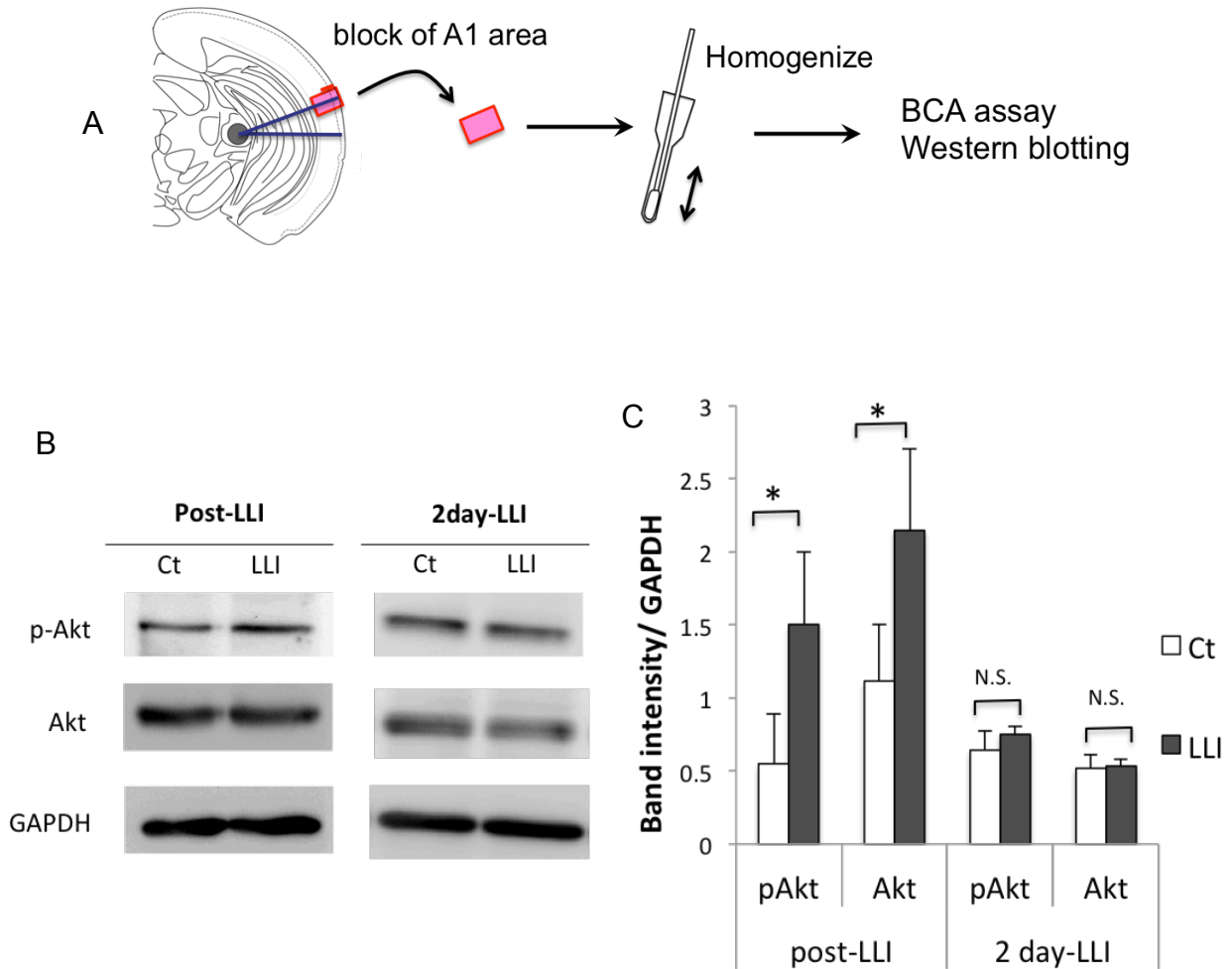


Fig. 24 Transcranial LLI effects on pAkt and Akt expression. A: schematic diagram of making sample in vivo. B: Western blot analysis of auditory cortex lysates at post-LLI and 2 days after LLI. GAPDH is a loading control. C: Quantification of blots using Image J. Band intensity was normalized to GAPDH (mean \pm SD, n = 4, t-test *p < 0.05).

5.4 Discussion

In the present studies (Chapters 4/5), we performed *in vivo* as well as *in vitro* experiments to reveal whether transcranial 532 nm LLI affects proliferation and migrating of GAD67-positive NSPCs in adult murine neocortex and also whether 532 nm LLI affects cultured NSPCs from embryonic mice. The *in vivo* experiments demonstrated that 532 nm LLI (60 mW) facilitated the migration of GABAergic neurons with a significant increase in Akt expression. Migration of GAD67-positive cells were also observed in the *in vitro* experiments, where 532 nm 60 min-LLI promoted the migrating of GAD67-positive NSPCs as well as the penetration beneath the trans-well membrane. These data suggest that LLI affects Akt expression and influences migration of GABAergic neurons derived from NSPCs.

It is well known that Akt plays an important role in the regulation of cellular processes that are critical for neuronal development, including gene transcription, cell proliferation, and neuronal migration. Souza et al. reported that dopamine D2 receptor activity modulates Akt signaling to promote GABAergic neurogenesis during development of zebrafish larvae¹⁰⁰). Oishi et al. demonstrated that active Akt promotes differentiation of telencephalic neural precursor cells into GABA-containing, but not glutamatergic, neurons¹⁰¹). Since these studies suggest a close relationship between Akt signaling activation and developing neural cell differentiation, it is likely that our finding of LLI effects on NSPCs is based on the Akt activation.

We found that 532 nm LLI increased pAkt and Akt after 4 hours compared with non-irradiated control but not after 2 days. Novoselova et al. showed 632.8 nm LLI increased the interleukin-2 (IL-2) production in T cells and IL-2 concentration in blood plasma within 1 day, whereas no significant difference was seen at 2 days after the laser treatment¹⁰²). These results suggest the effect of LLI on protein production is not permanent but temporary with a certain type of bystander effects¹⁰³). In addition, Akt expression was enhanced in both *in vivo* and *in vitro* experiments, but pAkt was only found *in vivo*. In our experiments, brain tissues include not only NSPCs but also other cells, whereas cultured cells include purified NSPCs grown as neurospheres. This difference in cell environment is one possible reason for the different observations in pAkt. However, further studies will be needed to understand the different effects of LLI between *in vivo* and *in vitro* systems.

A novel finding in this study is that 532 nm LLI promotes the migration of NSPCs into deeper layers of the neocortex. Functional nature of NSPCs is unclear. The mild ischemia in adult rats facilitated proliferation, differentiation and migration. Ohira et al. found that the newly generated neurons were GABAergic by GAD67 staining and that the neurons were functionally integrated into the neuronal circuitry as shown by activity-dependent c-Fos staining. Although we have not yet tried the c-Fos staining, which can detect responses to various physiological stimuli, future studies should investigate whether the migrated NSPCs induced by the LLI could be functionally integrated into cortical circuits.

The extent of LLI penetration into cortical tissues is worth discussing. The comparison to the control side of LLI in our experiments indicated direct LLI effects on the layer 1 NSPCs on the irradiated side. Although the possibility of LLI penetrating the brain from the irradiation site to the contralateral hemisphere (the control side) cannot be excluded completely, we suggest that 532 nm LLI could reach to deep layers at most, but not to the contralateral side at least 10 mm apart, because the penetration depth depends on LLI wavelength and LLI at short wavelength has low penetration depth^{104,105}). It was reported that the 1064 nm laser penetrates tissue (10 mm) twice as deep as the 830 nm laser (5 mm), and 10 times more than the 532 nm laser (0.8 mm)¹⁰⁶). Accordingly, the transcranial approach of 532 nm LLI used here is worthy of note, because of its possible application to various experiments in vivo.

Further, our findings regarding the promotion of the GABAergic NSPC migration by 532 nm LLI might also be valuable for clinical purpose. In the case of stroke, it is well known that excessive stimulation of synaptically-activated glutamate receptors leads to signaling toward neuronal cell death^{107, 108}). This excitotoxicity by tonic glutamatergic activities may be suppressed by 532 nm LLI-facilitated migration of GABAergic NSPCs before vulnerable brain regions become permanently damaged. Future studies will examine a dose-dependency of LLI (averaged power and irradiation time) to determine the most suitable transcranial approach.

5.5 References

- 100) Souza BR, Romano-Silva MA, Tropepe V (2011) Dopamine D2 receptor activity modulates Akt signaling and alters GABAergic neuron development and motor behavior in zebrafish larvae. *J Neuroscience* 31: 5512–5525.
- 101) Oishi K1, Watatani K, Itoh Y, Okano H, Guillemot F, et al. (2009) Selective induction of neocortical GABAergic neurons by the PDK1-Akt pathway through activation of Mash1. *Proc Natl Acad Sci USA* 106:13064–9.
- 102) Novoselova EG1, Glushkova OV, Cherenkov DA, Chudnovsky VM, Fesenko EE (2006) Effects of low-power laser radiation on mice immunity. *Photodermatol Photoimmunol Photomed* 22(1):33–8. PMID: 16436179
- 103) Huang D, Xiao T, Xu X, Tao D, Hu J, et al. (2008) Investigation of bystander effect in Molt-4 cells induced by ultraviolet ray. *Chinese-German J Clin Oncol* 7:227–229.
- 104) Staiger JF, Bisler S, Schleicher A, Gass P, Stehle JH, et al. (2000) Exploration of a novel environment leads to the expression of inducible transcription factors in barrel-related columns. *Neuroscience* 99: 7–16. PMID: 10924947
- 105) Rojas JC, Gonzalez-Lima F (2011) Low-level light therapy of the eye and brain. *Eye and Brain* 3, 49–67.
- 106) Te AE (2006) The Next Generation in Laser Treatments and the Role of the Green Light High-Performance System Laser. *Rev Urol.: 8 Suppl 3:S24–30*. PMID: 17173099
- 107) Rothman SM, Olney JW (1986) Glutamate and the pathophysiology of hypoxic-ischemic brain damage. *Ann Neurol* 19:105–111. PMID: 2421636
- 108) Choi DW (1992) Excitotoxic cell death. *J Neurobiol* 23:1261–1276. PMID: 1361523

Acknowledgment (謝辞)

本研究を論文として形にすることができたのは、温かくも厳しく多大なるご指導を頂きました木暮信一教授、川井秀樹准教授、山之端万里准教授のおかげです。研究を通して、先生から頂いた言葉は私の一生の宝です。

ともに研究に励みながら私に世界への視野を与えてくれた留学生の Ang Foong Yee さん、熱心で研究室への配慮を忘れない Hyeryun Shin さん、明るく常に努力をおしまない Minzi Chang さん、そして木暮研究室と川井研究室の皆様にもいつも元気と希望を頂いていました。ここに感謝を申し上げます。

大学院に進むことを応援してくれた家族には感謝を言葉では表しきれません。これから世界旅行へつれていくという親孝行の姿で表していきたいと思います。そして、悩んだ時は、ともに夢に向かって歩みつづけている親友の鈴木春香さん、鈴木樹璃さん、国井美恵子さんの言葉に支えられました。

研究支援を賜りました、笹川科学助成財団、内藤科学助成財団、日本学術振興会の関係者の皆様に感謝いたします。これよりまた研究に励み、助成して頂いた研究者としての責任を遂行して参ります。

最後に、いつも創大生を温かく見護ってくださる創価大学の創立者・池田大作先生に心より御礼申し上げます。「冬は必ず春となる」との言葉を胸に、世界へと躍進して自身の使命を果たして参ります。